Mathematics and Computers in Simulation 250 (2026) 423–441

Contents lists available at ScienceDirect

Mathematics and Computers in Simulation

journal homepage: www.elsevier.com/locate/matcom

Original articles

On G^2 interpolation by degree seven Minkowski Pythagorean-hodograph spline curves

Marjeta Knez [a,b], Francesca Pelosi [c], Maria Lucia Sampoli [c,*]

[a] FMF, University of Ljubljana, Jadranska 19, 1000 Ljubljana, Slovenia
[b] IMFM, Jadranska 19, 1000 Ljubljana, Slovenia
[c] Department of Information Engineering and Mathematics, University of Siena, Italy

ARTICLE INFO

Keywords:
Minkowski space
Minkowski Pythagorean-hodograph curves
Biarc curves
Geometric Hermite interpolation
Arc-length constraint
Spline construction

ABSTRACT

It is well established that curves in Minkowski space $\mathbb{R}^{2,1}$ are particularly well suited for representing the medial axis transform (MAT) of planar domains. In particular, Minkowski Pythagorean-hodograph (MPH) curves correspond to domains whose boundaries and offset curves are all rational (Moon, 1999). Motivated by recent results on G^2 Hermite interpolation by spatial PH curves (Knez et al., 2024), this paper extends that framework through the use of Clifford algebras. In more detail, we present the construction of a G^2 continuous MPH spline interpolant of degree seven, equipped with a rational G^1 continuous Lorentz orthonormal frame, under the additional constraint of a prescribed Minkowski length. To ensure applicability to arbitrary interpolation data, each spline segment is formed as a biarc composed of two polynomial MPH curves that match the geometric Hermite data at the endpoints. The proposed method is local and yields a closed-form solution with additional free parameters, where appropriate guidelines for their selection are given. Furthermore, two methods are proposed for determining the input frame data, where one is based on discrete point and derivative information, and the other introduces a novel approach that employs rotation-minimizing Lorentz frames, computed numerically via a generalization of the *double reflection method* (Wanget al., 2008) to Minkowski space. Several numerical experiments are included to demonstrate the effectiveness of the derived interpolation scheme and to show that the proposed parameter selection and frame data computation result in spline approximants with a high approximation order.

1. Introduction

Pythagorean-hodograph (PH) curves form an important subclass of polynomial parametric curves, characterized by the piecewise polynomial nature of their arc length function. In the planar case, they also admit rational offset curves. Since their introduction in [1], both planar and spatial PH curves have been extensively studied (see [2–4], and the references therein). Minkowski Pythagorean-hodograph (MPH) curves were later introduced in [5–7], motivated by the aim of representing segments of the medial axis transform of planar domains [8,9]. Recall that the medial axis of a planar domain is defined as the set of centers of all maximal inscribed circles that are tangent to the boundary at two or more points. The medial axis transform (MAT) is then constructed by lifting these points into (x, y, r)-space, where the radius of each corresponding circle serves as the third coordinate, forming a system of space curves.

* Corresponding author.
E-mail addresses: marjetka.knez@fmf.uni-lj.si (M. Knez), francesca.pelosi@unisi.it (F. Pelosi), marialucia.sampoli@unisi.it (M.L. Sampoli).

https://doi.org/10.1016/j.matcom.2026.06.035
Received 8 July 2025; Received in revised form 15 March 2026; Accepted 29 June 2026
Available online 8 July 2026

When the medial axis transform is composed of MPH curves, the boundary curve of the associated planar domain is a piecewise rational curve. A key advantage of this property is that it naturally extends to all offset curves of the boundary. Practical use of the offsets in tool path generation for Computer-Numerical-Control (CNC) machines and Computer-aided-manufacturing (CAM) requires a trimming process to remove extraneous segments. This step can be computationally demanding and time-consuming, depending on the curve's geometry and offset distance. As noted in [6], employing the medial axis transform representation can significantly simplify the trimming process for inner offsets, since only the parts of the MAT with circle radii smaller than the offset distance need to be removed.

This observation provides strong motivation for investigating approximation and interpolation techniques based on Minkowski Pythagorean-hodograph curves. The construction of PH and MPH curves from the so called *preimage* curves is based on quadratic representation formulas, so their generation from geometric data requires solving systems of quadratic equations. To avoid the computation of involved solutions, local constructions matching C^k or G^k Hermite boundary data appears to be the most promising. For example, G^1 Hermite interpolation using MPH cubics was studied in [10], while interpolation with MPH quintics was explored in [11]. The C^1 Hermite interpolation problem using MPH quartics was examined in [12], where the new concept of $C^{1/2}$ interpolation was introduced. Then a C^1 interpolation scheme based on MPH quintics was developed in [13]. In [14], an algorithm for C^2 Hermite interpolation employing MPH curves of degree nine was proposed. The idea of constructing the normal vector field — rather than the tangent — such that it satisfies the prescribed MPH conditions and matches the given first-order conditions was proposed in [15] and applied to G^1 Hermite interpolation with MPH quartics and C^1 Hermite interpolation with MPH quintics. Finally in [16,17] MPH B-spline curves were investigated.

In this paper, we aim to show that by using a suitable model based on the Clifford algebra many expressions and constructions for PH curves can be directly rewritten and applied to MPH curves. In particular, we study the construction of G^2 continuous MPH spline curves accompanied by G^1 continuous Lorentz orthonormal frames. In addition, a prescribed Minkowski length has to be matched. The proposed construction can be viewed as a generalization to MPH curves of the method presented in [18] for planar and [19] for spatial PH curves. The resulting interpolation scheme is entirely local and involves polynomial curve segments of degree seven. However, this approach leads to a highly nonlinear system that must be solved. To ensure that the scheme remains applicable to arbitrary interpolation data, we replace the polynomial segments with biarcs, which allows us to derive a closed-form solution for the interpolant. Due to the biarc splitting, the resulting interpolant includes additional free parameters, and their selection is suggested such that the biarc satisfies the length constraint and remains as close as possible to a single polynomial MPH interpolant. In addition, we propose two methods for determining the input frame data in the preimage space. The first method relies solely on discrete information about given points and their associated first and second order derivative vectors. The second introduces a novel approach that assigns to a given curve in the Minkowski space a rotation-minimizing Lorentz orthonormal frame, from which the required input data are derived. Specifically, *the double reflection method*, originally developed for curves in Euclidean space [20], is extended to the Minkowski setting, and a correspondence is established between frame vectors and elements of the Clifford algebra subspace (see Theorem 2). Numerical results indicate that the suggested choice of free parameters yields spline approximants with a high approximation order.

The remainder of this paper is organized as follows. Section 2 reviews fundamental concepts related to the Minkowski space, its associated Clifford algebra, the medial axis transform, and Minkowski Pythagorean-hodograph curves. The G^2 Hermite interpolation problem is presented in Section 3, while Section 4 explores two possible methods for computing the frame data. Section 5 presents several numerical examples to illustrate the results obtained using the proposed approach, and Section 6 contains the asymptotic analysis. The final section provides a brief summary and discusses potential directions for future work.

2. Short review on Minkowski Pythagorean-hodograph curves

2.1. Minkowski space $\mathbb{R}^{2,1}$ and MPH curves

Minkowski space $\mathbb{R}^{2,1}$ is a three–dimensional real vector space equipped with the Minkowski scalar product with the signature $(+,+,-)$, defined as

$$\langle \boldsymbol{x}, \boldsymbol{y}\rangle_{\mathrm{M}} = x_1 y_1 + x_2 y_2 - x_3 y_3 \quad \text{for} \quad \boldsymbol{x} = (x_1, x_2, x_3),\ \boldsymbol{y} = (y_1, y_2, y_3) \in \mathbb{R}^{2,1}.$$

The squared norm $\|\boldsymbol{x}\|^2_{\mathrm{M}} = \langle \boldsymbol{x}, \boldsymbol{x}\rangle_{\mathrm{M}}$ of a vector $\boldsymbol{x} \in \mathbb{R}^{2,1}$ can be positive, negative or zero, which classifies three types of vectors. Namely *space-like* if $\|\boldsymbol{x}\|^2_{\mathrm{M}} > 0$, *time-like* if $\|\boldsymbol{x}\|^2_{\mathrm{M}} < 0$, and *light-like* if $\|\boldsymbol{x}\|^2_{\mathrm{M}} = 0$. Moreover, the Minkowski cross product is defined as $\boldsymbol{x} \times_{\mathrm{M}} \boldsymbol{y} = (x_3 y_2 - x_2 y_3, x_1 y_3 - x_3 y_1, x_1 y_2 - x_2 y_1)$.

Definition 1. The polynomial curve $\boldsymbol{p} : [\alpha, \beta] \to \mathbb{R}^{2,1}$, $t \mapsto \boldsymbol{p}(t) = (x(t), y(t), r(t))$, is a Minkowski Pythagorean-hodograph curve (MPH curve) if

$$\|\boldsymbol{p}'(t)\|^2_{\mathrm{M}} = x'(t)^2 + y'(t)^2 - r'(t)^2 = \sigma(t)^2$$

for some polynomial function σ.

From the definition one can see that for MPH curves the hodograph vectors $\boldsymbol{p}'(t)$ cannot be *time-like* for any parameter $t \in [\alpha, \beta]$. MPH curves can be used for computing rational representation of the boundary of the given planar domain Ω through its medial axis transform. The *medial axis* of a planar domain $\Omega \subset \mathbb{R}^2$, denoted by $\mathrm{MA}(\Omega)$, is the locus of centers of maximal circles inscribed in the domain, i.e., circles that touch the boundary of the domain in at least two points. If for every maximal circle the radius is appended to its center position, this gives the so called *medial axis transform*

$$\mathrm{MAT}(\Omega) = \left\{(x, y, r) \in \Omega \times \mathbb{R}_0^+ \,:\, K_r(x, y) \text{ is maximal in } \Omega\right\},$$

where $K_r(x, y)$ denotes the circle with radius r and center in (x, y). The boundary of the domain Ω can be precisely reconstructed from its $\mathrm{MAT}(\Omega)$ using the envelope formula [21]

$$\begin{aligned}&(x^{\pm}_{\mathrm{env}}(t), y^{\pm}_{\mathrm{env}}(t)) = \\ &(x(t), y(t)) - \frac{r(t)}{x'(t)^2 + y'(t)^2}\left(r'(t)(x'(t), y'(t)) \mp \sqrt{x'(t)^2 + y'(t)^2 - r'(t)^2}(-y'(t), x'(t))\right).\end{aligned} \tag{1}$$

If the medial axis transform of a planar domain is parameterized by an MPH curve, then the envelopes are rational curves.

The construction of MPH curves is similar to that of spatial PH curves, where we can use the algebra of quaternions to get a compact representation. The algebra behind MPH curves is the Clifford algebra $Cl(2,1)$, which we briefly review in the next subsection (see [7] for further details).

2.2. Clifford algebra $Cl(2,1)$ and its subalgebra $\mathbb{A}$

To construct MPH curves we need the Clifford algebra $Cl(2,1)$, which is an 8-dimensional vector space with the basis $\{\mathbf{1}, \boldsymbol{e}_1, \boldsymbol{e}_2, \boldsymbol{e}_3, \boldsymbol{e}_{12}, \boldsymbol{e}_{23}, \boldsymbol{e}_{31}, \boldsymbol{e}_{123}\}$, where the multiplication rules between the generators $\boldsymbol{e}_1$, $\boldsymbol{e}_2$, $\boldsymbol{e}_3$ are given by:

- $\boldsymbol{e}_i\boldsymbol{e}_j = -\boldsymbol{e}_j\boldsymbol{e}_i$ for all $i \neq j$;
- $\boldsymbol{e}_1^2 = 1, \quad \boldsymbol{e}_2^2 = 1, \quad \boldsymbol{e}_3^2 = -1.$

In addition the product of generators is denoted by $\boldsymbol{e}_{i_1}\boldsymbol{e}_{i_2}\cdots\boldsymbol{e}_{i_k} = \boldsymbol{e}_{i_1 i_2\ldots i_k}$ and we set $\boldsymbol{e}_\emptyset = \mathbf{1}$. Every $\mathcal{A} \in Cl(2,1)$ can be written as

$$\mathcal{A} = a_0\mathbf{1} + a_1\boldsymbol{e}_1 + a_2\boldsymbol{e}_2 + a_3\boldsymbol{e}_3 + a_4\boldsymbol{e}_{12} + a_5\boldsymbol{e}_{23} + a_6\boldsymbol{e}_{31} + a_7\boldsymbol{e}_{123} \equiv (a_0, a_1, a_2, a_3, a_4, a_5, a_6, a_7).$$

The coefficient a_0 is called a scalar part of $\mathcal{A}$. Elements with $a_0 = a_4 = a_5 = a_6 = a_7 = 0$ are called *pure vectors*. We connect this algebra with the Minkowski space $\mathbb{R}^{2,1}$ by identifying $\mathbb{R}^{2,1} \equiv \mathbb{R}\,\boldsymbol{e}_1 + \mathbb{R}\,\boldsymbol{e}_2 + \mathbb{R}\,\boldsymbol{e}_3$. Namely, pure vectors are identified with vectors in $\mathbb{R}^{2,1}$. The conjugate element and the squared Clifford norm of $\mathcal{A} \in Cl(2,1)$ are computed as

$$\begin{aligned}&\overline{\mathcal{A}} = (a_0, -a_1, -a_2, -a_3, -a_4, -a_5, -a_6, a_7),\\ &N(\mathcal{A}) = \mathcal{A}\overline{\mathcal{A}} = \left(a_0^2 - a_1^2 - a_2^2 + a_3^2 + a_4^2 - a_5^2 - a_6^2 + a_7^2\right)\mathbf{1} + 2\left(a_0a_7 - a_1a_5 - a_2a_6 - a_3a_4\right)\boldsymbol{e}_{123}.\end{aligned}$$

More generally, we define $N(\mathcal{A}, \mathcal{B}) = \frac{1}{2}(\mathcal{A}\overline{\mathcal{B}} + \mathcal{B}\overline{\mathcal{A}})$, and observe that $N(\mathcal{A}) = N(\mathcal{A}, \mathcal{A})$.

We denote by $\mathbb{A} = \mathbb{R}\,\mathbf{1} + \mathbb{R}\,\boldsymbol{e}_{12} + \mathbb{R}\,\boldsymbol{e}_{23} + \mathbb{R}\,\boldsymbol{e}_{31}$ the subalgebra of $Cl(2,1)$. The product between $\mathcal{A} = a_0\mathbf{1} + a_4\boldsymbol{e}_{12} + a_5\boldsymbol{e}_{23} + a_6\boldsymbol{e}_{31} \in \mathbb{A}$ and $\mathcal{B} = b_0\mathbf{1} + b_4\boldsymbol{e}_{12} + b_5\boldsymbol{e}_{23} + b_6\boldsymbol{e}_{31} \in \mathbb{A}$ equals $\mathcal{A}\,\mathcal{B} = \mathcal{C} = c_0\mathbf{1} + c_4\boldsymbol{e}_{12} + c_5\boldsymbol{e}_{23} + c_6\boldsymbol{e}_{31}$, where

$$\begin{aligned}&c_0 = a_0b_0 - a_4b_4 + a_5b_5 + a_6b_6, \quad c_4 = a_4b_0 + a_0b_4 - a_6b_5 + a_5b_6,\\ &c_5 = a_5b_0 - a_6b_4 + a_0b_5 + a_4b_6, \quad c_6 = a_6b_0 + a_5b_4 - a_4b_5 + a_0b_6,\end{aligned}$$

and the squared Clifford norm of $\mathcal{A}$ is a scalar value $N(\mathcal{A}) = \left(a_0^2 + a_4^2 - a_5^2 - a_6^2\right)\mathbf{1}$. Similarly, we compute that $N(\mathcal{A}, \mathcal{B}) = \left(a_0b_0 + a_4b_4 - a_5b_5 - a_6b_6\right)\mathbf{1}$, so in what follows we identify $N(\mathcal{A})$ and $N(\mathcal{A}, \mathcal{B})$ with real numbers. In further computations we use also the standard L^2 norm, defined in a classical way by identifying $Cl(2,1)$ with 8-dimensional vector space, i.e., $\|\mathcal{A}\|_2 = \sqrt{\sum_{j=0}^7 a_j^2}$. The following operation is essential for the construction of MPH curves.

Definition 2. We define the operation $\star : \mathbb{A} \times \mathbb{A} \to \mathbb{R}^{2,1}$ by $\mathcal{A} \star \mathcal{B} := \frac{1}{2}\left(\mathcal{A}\,\boldsymbol{e}_1\overline{\mathcal{B}} + \mathcal{B}\boldsymbol{e}_1\overline{\mathcal{A}}\right) \equiv \boldsymbol{c} = (c_1, c_2, c_3)$,

$$(c_1, c_2, c_3) := \left(a_0b_0 - a_4b_4 - a_5b_5 + a_6b_6, -a_4b_0 - a_0b_4 - a_6b_5 - a_5b_6, a_6b_0 + a_5b_4 + a_4b_5 + a_0b_6\right).$$

Moreover, $\mathcal{A}^{2\star} = \mathcal{A} \star \mathcal{A} \equiv \left(a_0^2 - a_4^2 - a_5^2 + a_6^2, -2\left(a_0a_4 + a_5a_6\right), 2\left(a_4a_5 + a_0a_6\right)\right)$.

The solutions of the quadratic $\star$-equation $\mathcal{X}^{2\star} = \boldsymbol{c}$ and the linear $\star$-equation $\mathcal{X} \star \mathcal{A} = \boldsymbol{c}$, which will further be needed, are given in the next two lemmas, proven in [13].

Lemma 1. *Let $\boldsymbol{c} = (c_1, c_2, c_3) \in \mathbb{R}^{2,1}$ be a given nonzero space-like vector. Then the solutions $\mathcal{X} \in \mathbb{A}$ of the equation $\mathcal{X}^{2\star} = \boldsymbol{c}$ depend on one free parameter ϕ and are of four different types. Namely,*

$$\mathcal{X} = \mathcal{X}(\ell, \phi) = \sqrt[\star]{\boldsymbol{c}}\,\mathcal{W}(\ell, \phi), \quad \ell = 1, 2, 3, 4,$$

where

$$\begin{aligned}&\mathcal{W}(1, \phi) := (\cosh(\phi), 0, 0, 0, 0, -\sinh(\phi), 0, 0), \quad \mathcal{W}(2, \phi) := (-\cosh(\phi), 0, 0, 0, 0, -\sinh(\phi), 0, 0),\\ &\mathcal{W}(3, \phi) := (0, 0, 0, 0, -\sinh(\phi), 0, -\cosh(\phi), 0), \quad \mathcal{W}(4, \phi) := (0, 0, 0, 0, -\sinh(\phi), 0, \cosh(\phi), 0),\end{aligned}$$

and

$$\sqrt[\star]{\boldsymbol{c}} := \begin{cases} \frac{1}{2\sqrt{\alpha(\boldsymbol{c})}}\left(c_3,0,0,0,0,-c_2,2\alpha(\boldsymbol{c}),0\right), & \alpha(\boldsymbol{c})>0 \\ \frac{1}{2\sqrt{-\alpha(\boldsymbol{c})}}\left(0,0,0,0,c_3,-2\alpha(\boldsymbol{c}),-c_2,0\right), & \alpha(\boldsymbol{c})<0 \\ \left(-c_2,0,0,0,\frac{1}{4}-c_1,c_3,-\operatorname{sign}(c_2c_3)\left(\frac{1}{4}+c_1\right),0\right), & \alpha(\boldsymbol{c})=0,\ c_2c_3\neq 0, \\ \left(0,0,0,0,\frac{1}{4}-c_1,0,\frac{1}{4}+c_1,0\right), & \alpha(\boldsymbol{c})=0,\ c_2=c_3=0 \end{cases}$$

where $\alpha(\boldsymbol{c}) := \frac{1}{2}\left(c_1+\sqrt{c_1^2+c_2^2-c_3^2}\right)$.

Remark 1. It is straightforward to compute that $N(\sqrt[\star]{\boldsymbol{c}}) = -\|\boldsymbol{c}\|_{\mathrm{M}}$ for $\alpha(\boldsymbol{c})>0$, and $N(\sqrt[\star]{\boldsymbol{c}}) = \|\boldsymbol{c}\|_{\mathrm{M}}$ for $\alpha(\boldsymbol{c})\le 0$.

Remark 2. Note that $N(\mathcal{W}(1,\phi)) = N(\mathcal{W}(2,\phi)) = 1$ and $N(\mathcal{W}(3,\phi)) = N(\mathcal{W}(4,\phi)) = -1$. Furthermore, $\mathcal{W}(1,\phi) = -\mathcal{W}(2,-\phi)$ and $\mathcal{W}(3,\phi) = -\mathcal{W}(4,-\phi)$ for every $\phi\in\mathbb{R}$.

Lemma 2. *Let* $\boldsymbol{c}=(c_1,c_2,c_3)\in\mathbb{R}^{2,1}$ *be a given vector and* $\mathcal{A}=(a_0,0,0,0,a_4,a_5,a_6,0)\in\mathbb{A}$ *such that* $N(\mathcal{A})\neq 0$. *Then all the solutions* $\mathcal{X}\in\mathbb{A}$ *of the linear equation* $\mathcal{X}\star\mathcal{A}=\boldsymbol{c}$ *are expressed with one free parameter* $\zeta\in\mathbb{R}$ *as*

$$\mathcal{X}=\mathcal{X}(\zeta)=\frac{1}{N(\mathcal{A})}\left(c_1\boldsymbol{e}_1+c_2\boldsymbol{e}_2+c_3\boldsymbol{e}_3+\zeta\boldsymbol{e}_{123}\right)\mathcal{A}\boldsymbol{e}_1.$$

2.3. Construction of MPH curves

To construct polynomial MPH curves, introduced in Definition 1, we take $\mathbb{A}$ as the so called *preimage* space. By $\mathbb{P}_m[\mathbb{A}]$, $m\in\mathbb{N}_0$, we denote the space of (univariate) polynomials of degree m with coefficients from $\mathbb{A}$. We call these polynomials the *preimage* polynomials. Choosing $\mathcal{A}\in\mathbb{P}_m[\mathbb{A}]$, $\mathcal{A}=(a_0,0,0,0,a_4,a_5,a_6,0)$, for some chosen degree $m\ge 1$ and computing $\boldsymbol{h}=\mathcal{A}^{2\star}\in\mathbb{P}_{2m}[\mathbb{R}^{2,1}]$, we get by $\boldsymbol{p}(t)=\int_\tau^t \boldsymbol{h}(\xi)d\xi+\boldsymbol{c}$, $\boldsymbol{c}=\mathrm{const}\in\mathbb{R}^{2,1}$, $\tau\in\mathbb{R}$, a parametric curve that satisfies

$$\sigma^2(t)=\|\boldsymbol{p}'(t)\|_{\mathrm{M}}^2=N(\mathcal{A}(t))^2.$$

More precisely,

$$\sigma(t)=\|\boldsymbol{p}'(t)\|_{\mathrm{M}}=\sqrt{(a_0^2(t)+a_4^2(t)-a_5^2(t)-a_6^2(t))^2}=\left|a_0^2(t)+a_4^2(t)-a_5^2(t)-a_6^2(t)\right|$$

and $N(\mathcal{A}(t))=a_0^2(t)+a_4^2(t)-a_5^2(t)-a_6^2(t)$, thus the curve $\boldsymbol{p}$ is an MPH curve of degree $2m+1$ with the hodograph $\boldsymbol{h}$. Assuming that $N(\mathcal{A}(t))$ does not change sign on the parameter interval, σ is a polynomial of degree $2m$, and we call $\boldsymbol{p}$ a *regular* MPH curve. In [7] it is proven that the condition on the choice of the hodograph is sufficient and necessary, so any MPH curve can be constructed in this way. For irregular MPH curves, σ is a piecewise polynomial $\sigma(t)=|N(\mathcal{A})(t)|$.

In what follows we consider MPH curves of degree 7 parameterized on the interval $[\tau,\tau+\Delta\tau]$, $\Delta\tau>0$. The preimage polynomial is thus of degree 3, and we express it using the Bernstein basis polynomials $B_i^m(t):=\binom{m}{i}t^i(1-t)^{m-i}$, $i=0,1,\dots,m$, as

$$\mathcal{A}(t)=\sum_{i=0}^{3}\mathcal{A}_iB_i^3\left(\frac{t-\tau}{\Delta\tau}\right),\quad \mathcal{A}_i\in\mathbb{A}. \tag{2}$$

Then

$$\boldsymbol{h}(t)=\mathcal{A}(t)\star\mathcal{A}(t)=\sum_{i=0}^{6}\boldsymbol{h}_iB_i^6\left(\frac{t-\tau}{\Delta\tau}\right)\quad\text{and}\quad \boldsymbol{p}(t)=\sum_{i=0}^{7}\boldsymbol{p}_iB_i^7\left(\frac{t-\tau}{\Delta\tau}\right), \tag{3}$$

where

$$\begin{aligned} &\boldsymbol{h}_0=\mathcal{A}_0^{2\star},\quad \boldsymbol{h}_1=\mathcal{A}_0\star\mathcal{A}_1,\quad \boldsymbol{h}_2=\frac{1}{5}\left(2\mathcal{A}_0\star\mathcal{A}_2+3\mathcal{A}_1^{2\star}\right),\quad \boldsymbol{h}_3=\frac{1}{10}\left(\mathcal{A}_0\star\mathcal{A}_3+9\mathcal{A}_1\star\mathcal{A}_2\right),\\ &\boldsymbol{h}_4=\frac{1}{5}\left(2\mathcal{A}_1\star\mathcal{A}_3+3\mathcal{A}_2^{2\star}\right),\quad \boldsymbol{h}_5=\mathcal{A}_2\star\mathcal{A}_3,\quad \boldsymbol{h}_6=\mathcal{A}_3^{2\star}, \end{aligned} \tag{4}$$

and

$$\boldsymbol{p}_{i+1}=\boldsymbol{p}_0+\frac{\Delta\tau}{7}\sum_{j=0}^{i}\boldsymbol{h}_j,\quad i=0,1,\dots,6. \tag{5}$$

Moreover, $\sigma(t)=|N(\mathcal{A}(t))|=\left|\sum_{i=0}^{6}\sigma_iB_i^6\left(\frac{t-\tau}{\Delta\tau}\right)\right|$, where

$$\sigma_0=N(\mathcal{A}_0),\quad \sigma_1=N(\mathcal{A}_0,\mathcal{A}_1),\quad \sigma_2=\frac{1}{5}\left(2N(\mathcal{A}_0,\mathcal{A}_2)+3N(\mathcal{A}_1)\right),\quad \sigma_3=\frac{1}{10}\left(N(\mathcal{A}_0,\mathcal{A}_3)+9N(\mathcal{A}_1,\mathcal{A}_2)\right),$$

$$\sigma_4 = \frac{1}{5}\left(2N(\mathcal{A}_1,\mathcal{A}_3)+3N(\mathcal{A}_2)\right), \quad \sigma_5 = N(\mathcal{A}_2,\mathcal{A}_3), \quad \sigma_6 = N(\mathcal{A}_3). \tag{6}$$

Further, we define the Minkowski length

$$\mathrm{length}_{\mathrm{M}}(\boldsymbol{p};[\tau,\tau+\Delta\tau]) := \int_{\tau}^{\tau+\Delta\tau} \left\|\boldsymbol{p}'(t)\right\|_{\mathrm{M}} dt,$$

which can be for regular MPH curves explicitly computed as

$$\mathrm{length}_{\mathrm{M}}(\boldsymbol{p};[\tau,\tau+\Delta\tau]) = \frac{\Delta\tau}{7}\left|\sum_{i=0}^{6}\sigma_i\right|.$$

2.4. Minkowski orthonormal frames and geometric continuity

We observe that for every $\mathcal{A}\in\mathbb{A}$ the products $\mathcal{A}\boldsymbol{e}_j\overline{\mathcal{A}}$, $j=1,2,3$, lie in the subspace $\mathbb{R}\boldsymbol{e}_1+\mathbb{R}\boldsymbol{e}_2+\mathbb{R}\boldsymbol{e}_3$, that we identify with $\mathbb{R}^{2,1}$. Hence, with every $\mathcal{A}\in\mathbb{A}$, such that $N(\mathcal{A})\neq 0$, we can associate a triple $\left(\boldsymbol{l}_1,\boldsymbol{l}_2,\boldsymbol{l}_3\right)$ of elements in $\mathbb{R}^{2,1}$, defined as

$$\boldsymbol{l}_1 = \frac{\mathcal{A}\boldsymbol{e}_1\overline{\mathcal{A}}}{N(\mathcal{A})}, \quad \boldsymbol{l}_2 = \frac{\mathcal{A}\boldsymbol{e}_2\overline{\mathcal{A}}}{N(\mathcal{A})}, \quad \boldsymbol{l}_3 = \frac{\mathcal{A}\boldsymbol{e}_3\overline{\mathcal{A}}}{N(\mathcal{A})},$$

which are such that $\left\langle \boldsymbol{l}_i,\boldsymbol{l}_j\right\rangle_{\mathrm{M}} = \delta_{i,j}$ for $i\neq j$, and $\langle \boldsymbol{l}_1,\boldsymbol{l}_1\rangle_{\mathrm{M}} = \langle \boldsymbol{l}_2,\boldsymbol{l}_2\rangle_{\mathrm{M}} = -\langle \boldsymbol{l}_3,\boldsymbol{l}_3\rangle_{\mathrm{M}} = 1$. i.e., they form an orthonormal basis of $\mathbb{R}^{2,1}$ with respect to the Minkowski scalar product. Taking these elements as columns of a 3×3 matrix $\mathcal{L}(\mathcal{A})$, the corresponding linear mapping $\mathcal{L}(\mathcal{A}):\mathbb{R}^{2,1}\to\mathbb{R}^{2,1}$ is called a Lorentz transform. The matrix $\mathcal{L}(\mathcal{A})$ is an element of a Lorentz group $\mathrm{SO}(2,1)$ (see [22] for more details), and it can be checked that $\det\mathcal{L}(\mathcal{A})=1$. This observation implies the following definition.

Definition 3. With every preimage polynomial $\mathcal{A}\in\mathbb{P}_m[\mathbb{A}]$, such that $N(\mathcal{A}(t))\neq 0$, we associate a Lorentz-Minkowski ON frame $\mathcal{L}(\mathcal{A};t) := \mathcal{L}(\mathcal{A}(t)) := (\boldsymbol{l}_1(t),\boldsymbol{l}_2(t),\boldsymbol{l}_3(t))$, where $\boldsymbol{l}_j(t) = \frac{\mathcal{A}(t)\boldsymbol{e}_j\overline{\mathcal{A}}(t)}{N(\mathcal{A}(t))}$.

Following [23], we define the notion of geometric continuity for frames.

Definition 4. Let $\mathcal{Q}_1 : I_1\subset\mathbb{R}\to\mathbb{A}$ and $\mathcal{Q}_2 : I_2\subset\mathbb{R}\to\mathbb{A}$ be given, such that $N(\mathcal{Q}_j(t))\neq 0$ for $t\in I_j$, $j=1,2$, and let $\mathcal{L}_1=\mathcal{L}(\mathcal{Q}_1;\cdot)$ and $\mathcal{L}_2=\mathcal{L}(\mathcal{Q}_2;\cdot)$ be the corresponding Lorentz ON frames. Assume that $\mathcal{L}_1(\tau_1)=\mathcal{L}_2(\tau_2)$ for some $\tau_1\in I_1$ and $\tau_2\in I_2$. Then the frames are G^k continuous at $\mathcal{L}_1(\tau_1)=\mathcal{L}_2(\tau_2)$ iff in some small interval around τ_1 there exist a scalar function λ and a regular reparameterization function φ, such that $\lambda(\tau_1)\neq 0$, $\varphi(\tau_1)=\tau_2$, $\varphi'(\tau_1)>0$, and the conditions

$$\frac{d^j}{dt^j}\mathcal{Q}_1(t)\Big|_{t=\tau_1} = \frac{d^j}{dt^j}\left(\lambda(t)\mathcal{Q}_2(\varphi(t))\right)\Big|_{t=\tau_1}, \quad j=0,1,\dots,k, \tag{7}$$

hold true.

The next theorem follows by the same arguments as in [23].

Theorem 1. *Recall Definition 4 and let $\boldsymbol{p}_1 : I_1\to\mathbb{R}^{2,1}$ and $\boldsymbol{p}_2 : I_2\to\mathbb{R}^{2,1}$ be two MPH curves with hodographs equal to $\mathcal{Q}_j^{2\star}$, $j=1,2$. Assume further that $\boldsymbol{p}_1(\tau_1)=\boldsymbol{p}_2(\tau_2)$, and that the G^k continuity conditions (7) are satisfied, where λ is connected with φ as*

$$\varphi^{(j+1)}(\tau_1) = \frac{d^j}{dt^j}\left(\lambda^2(t)\right)\Big|_{t=\tau_1}, \quad j=0,1\dots,k. \tag{8}$$

Then with this reparameterization function φ, the conditions

$$\frac{d^j}{dt^j}\boldsymbol{p}_1(t)\Big|_{t=\tau_1} = \frac{d^j}{dt^j}\boldsymbol{p}_2(\varphi(t))\Big|_{t=\tau_1} \tag{9}$$

for $j=0,1,\dots,k+1$ are satisfied, which implies the G^{k+1} continuity between $\boldsymbol{p}_1$ and $\boldsymbol{p}_2$ at the joint point.

Using (8), the conditions (7) and (9) for G^2 continuity of MPH curves are equal to

$$\mathcal{Q}_1(\tau_1)=\lambda(\tau_1)\mathcal{Q}_2(\tau_2), \quad \mathcal{Q}_1'(\tau_1)=\lambda'(\tau_1)\mathcal{Q}_2(\tau_2)+\lambda^3(\tau_1)\mathcal{Q}_2'(\tau_2), \quad \text{and}$$
$$\boldsymbol{p}_1(\tau_1)=\boldsymbol{p}_2(\tau_2), \quad \boldsymbol{p}_1'(\tau_1)=\lambda^2(\tau_1)\boldsymbol{p}_2'(\tau_2), \quad \boldsymbol{p}_1''(\tau_1)=2\lambda(\tau_1)\lambda'(\tau_1)\boldsymbol{p}_2'(\tau_2)+\lambda^4(\tau_1)\boldsymbol{p}_2''(\tau_2),$$

where $\boldsymbol{p}_j' = \mathcal{Q}_j^{2\star}$ and $\boldsymbol{p}_j'' = 2\mathcal{Q}_j\star\mathcal{Q}_j'$, $j=1,2$. Based on these equalities, we can define the G^2 interpolation problem by replacing the values $\mathcal{Q}_2(\tau_2)$, $\mathcal{Q}_2'(\tau_2)$ with interpolation data and taking $\lambda(\tau_1)$, $\lambda'(\tau_1)$ as free parameters.

3. Construction of G^2 continuous MPH curves

In this section, we introduce and analyze an interpolation problem for constructing G^2 continuous MPH spline curves that are equipped with G^1 continuous Lorentz ON frame, and have a prescribed Minkowski length. The presented construction generalizes to MPH curves the method studied in [18] for planar and in [19] for spatial PH curves.

3.1. Interpolation data and interpolation equations

Suppose that we are given the following interpolation data:

1. data points $\boldsymbol{P}_j \in \mathbb{R}^{2,1}$, $j = 0, 1, \ldots, J$;
2. preimage points/frame data $\mathcal{U}_j \in \mathbb{A}$, $j = 0, 1, \ldots, J$;
3. preimage derivatives/frame velocity data $\mathcal{V}_j \in \mathbb{A}$, $j = 0, 1, \ldots, J$;
4. length's increases ΔL_j, $j = 0, 1, \ldots, J-1$.

Without losing generality, we assume that $N(\mathcal{U}_j) > 0$, $j = 0, 1, \ldots, J$. Moreover, let $\tau_0 < \tau_1 < \cdots < \tau_{J-1} < \tau_J$ be the chosen interpolation parameters that split the interval $[\tau_0, \tau_J]$ into J segments. Since the geometric continuity is independent of the parameterization, we can assume that the parameters τ_j are equidistant. The goal is to construct the MPH spline $\boldsymbol{s} : [\tau_0, \tau_J] \to \mathbb{R}^{2,1}$ of degree 7 with breakpoints $(\tau_j)_{j=0}^J$ that has the preimage $\mathcal{A}_s : [\tau_0, \tau_J] \to \mathbb{A}$ of degree 3 and satisfies the interpolation conditions

$$\boldsymbol{s}(\tau_j) = \boldsymbol{P}_j, \quad \mathcal{A}_s(\tau_j) = \lambda_j \mathcal{U}_j, \quad \mathcal{A}_s'(\tau_j) = \lambda_{j,1}\mathcal{U}_j + \lambda_j^3 \mathcal{V}_j, \quad j = 0, 1, \ldots, J, \quad \text{and} \tag{10a}$$

$$\mathrm{length}_{\mathrm{M}}(\boldsymbol{s}; [\tau_j, \tau_{j+1}]) = \Delta L_j, \quad j = 0, 1, \ldots, J-1, \tag{10b}$$

for some yet unknown real values $\lambda_j > 0$ and $\lambda_{j,1}$, i.e., it interpolates the given data in a G^2 sense as explained in Definition 4 and in Theorem 1.

Remark 3. Since

$$\boldsymbol{s}'(\tau_j) = \mathcal{A}_s^{2\star}(\tau_j) = \lambda_j^2 \mathcal{U}_j^{2\star}, \quad \boldsymbol{s}''(\tau_j) = 2\mathcal{A}_s(\tau_j) \star \mathcal{A}_s'(\tau_j) = 2\lambda_j \lambda_{j,1} \mathcal{U}_j^{2\star} + \lambda_j^4 (2\,\mathcal{U}_j \star \mathcal{V}_j),$$

the spline $\boldsymbol{s}$ approximates the tangent vectors $\boldsymbol{t}_j = \mathcal{U}_j^{2\star}$ and the second-order derivative vectors $\boldsymbol{d}_j = 2\,\mathcal{U}_j \star \mathcal{V}_j$ in the G^2 sense.

Remark 4. Note that changing

$$\mathcal{U}_j \to \frac{\mathcal{U}_j}{\left\|\mathcal{U}_j\right\|}, \quad \mathcal{V}_j \to \frac{\mathcal{V}_j}{\left\|\mathcal{U}_j\right\|^3}, \quad \lambda_j \to \lambda_j \left\|\mathcal{U}_j\right\|, \quad \lambda_{j,1} \to \lambda_{j,1} \left\|\mathcal{U}_j\right\|$$

does not change conditions (10).

The straightforward approach is to take $\boldsymbol{s}|_{[\tau_j,\tau_{j+1}]}$ as a polynomial MPH curve of degree 7 with the corresponding cubic preimage curve $\mathcal{A}_s|_{[\tau_j,\tau_{j+1}]}$ for each $j = 0, 1, \ldots, J-1$. In this way, the spline $\boldsymbol{s}$ is globally G^2 continuous and the construction is completely local. But, as shown in the next subsection, the Eqs. (10) lead to a highly nonlinear system to be solved. So, as an alternative approach we propose to take $\boldsymbol{s}|_{[\tau_j,\tau_{j+1}]}$ to be a biarc composed of two polynomial MPH segments. Due to the locality, we limit the analysis in the next two subsections to only one segment — the first one.

3.2. Single polynomial MPH interpolant

Let $\boldsymbol{p} = \boldsymbol{s}|_{[\tau_0,\tau_1]}$, $\boldsymbol{h} = \boldsymbol{s}'|_{[\tau_0,\tau_1]}$ and $\mathcal{A} = \mathcal{A}_s|_{[\tau_0,\tau_1]}$ be expressed as in (2) and (3) with $\tau = \tau_0$ and $\Delta\tau = \tau_1 - \tau_0 =: \Delta\tau_0$.
From the second and the third condition in (10a) it follows that

$$\mathcal{A}_0 = \lambda_0\,\mathcal{U}_0, \quad \mathcal{A}_1 = \mu_0\,\mathcal{U}_0 + \frac{\Delta\tau_0}{3}\lambda_0^3\,\mathcal{V}_0, \quad \mathcal{A}_2 = \mu_1\,\mathcal{U}_1 - \frac{\Delta\tau_0}{3}\lambda_1^3\,\mathcal{V}_1, \quad \mathcal{A}_3 = \lambda_1\,\mathcal{U}_1,$$

where $\mu_0 := \lambda_0 + \frac{\Delta\tau_0}{3}\lambda_{0,1}$, $\mu_1 := \lambda_1 - \frac{\Delta\tau_0}{3}\lambda_{1,1}$. The point interpolation condition gives $\boldsymbol{p}_0 = \boldsymbol{P}_0$ and

$$\begin{aligned}\frac{7}{\Delta\tau_0}\Delta\boldsymbol{P}_0 =& \mathcal{A}_0^{2\star} + \mathcal{A}_0 \star \mathcal{A}_1 + \frac{1}{5}\left(2\mathcal{A}_0 \star \mathcal{A}_2 + 3\mathcal{A}_1^{2\star}\right) + \frac{1}{10}\left(\mathcal{A}_0 \star \mathcal{A}_3 + 9\mathcal{A}_1 \star \mathcal{A}_2\right)\\ &+ \frac{1}{5}\left(2\mathcal{A}_1 \star \mathcal{A}_3 + 3\mathcal{A}_2^{2\star}\right) + \mathcal{A}_2 \star \mathcal{A}_3 + \mathcal{A}_3^{2\star},\end{aligned}$$

where $\Delta\boldsymbol{P}_0 = \boldsymbol{P}_1 - \boldsymbol{P}_0$, which together with length interpolation equation (10b),

$$\begin{aligned}\frac{7}{\Delta\tau_0}\Delta L_0 =& N(\mathcal{A}_0) + N(\mathcal{A}_0, \mathcal{A}_1) + \frac{1}{5}\left(2N(\mathcal{A}_0, \mathcal{A}_2) + 3N(\mathcal{A}_1)\right) + \frac{1}{10}\left(N(\mathcal{A}_0, \mathcal{A}_3) + 9N(\mathcal{A}_1, \mathcal{A}_2)\right)\\ &+ \frac{1}{5}\left(2N(\mathcal{A}_1, \mathcal{A}_3) + 3N(\mathcal{A}_2)\right) + N(\mathcal{A}_2, \mathcal{A}_3) + N(\mathcal{A}_3),\end{aligned}$$

provided that $N(\mathcal{A}(t)) > 0$, lead to a highly nonlinear system of four equations for four unknowns $\lambda_0, \lambda_1, \mu_0, \mu_1$. Since the system is too involved for algebraic solvers (e.g. `Solve` function in Mathematica), the only way to numerically compute the solution is to use some iterative methods like Newton–Raphson method. This requires to choose good starting values, which is a nontrivial task. The numerical examples in Section 5 demonstrate that the biarc MPH interpolants, introduced in the following subsection, offer an excellent alternative with various advantages.

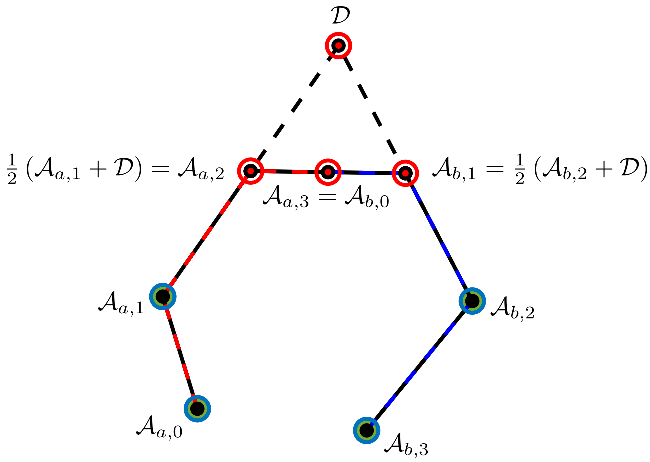

Fig. 1. Geometric illustration of super-smoothness of order 2 for the preimage Bézier coefficients.

3.3. Biarc MPH interpolant

Replacing a single polynomial curve with two polynomial biarc segments is a common way to introduce additional degrees of freedom into the interpolation problem while preserving the same polynomial degree. A polynomial biarc curve defined over the interval $[\tau_0, \tau_1]$, with the split point $\frac{\tau_0+\tau_1}{2}$, consists of two polynomial curves defined on the corresponding subintervals. To simplify the construction and avoid an unnecessary increase in the number of degrees of freedom, it is customary to impose a higher order of continuity between the two segments at the split parameter. We apply this idea in the following construction as well. In our case, the MPH interpolant on $[\tau_0, \tau_1]$ is constructed as a *biarc*, where both subsegments are represented by polynomial Bézier curves of degree 7, derived from preimages of degree 3.

The idea here is to impose C^2 *super-smoothness* on $\mathcal{A}$ at the midpoint. This removes any visible joint inside the segment and significantly reduces the degrees of freedom by enforcing simple algebraic relations between the Bézier control points of the two arc segments.

In more detail, let $\boldsymbol{p} = \boldsymbol{s}|_{[\tau_0,\tau_1]}$, $\boldsymbol{h} = \boldsymbol{s}'|_{[\tau_0,\tau_1]}$ and $\mathcal{A} = \mathcal{A}_s|_{[\tau_0,\tau_1]}$ be chosen as biarc curves of the form

$$\begin{aligned}
\boldsymbol{p}(t) &= \begin{cases} \boldsymbol{p}_a(t), & t \in \left[\tau_0, \frac{\Delta\tau_0}{2}\right) \\ \boldsymbol{p}_b(t), & t \in \left[\frac{\Delta\tau_0}{2}, \tau_1\right], \end{cases} \quad \boldsymbol{p}_a(t) = \sum_{i=0}^{7} \boldsymbol{p}_{a,i} B_i^7\left(\frac{2t-2\tau_0}{\Delta\tau_0}\right), \quad \boldsymbol{p}_b(t) = \sum_{i=0}^{7} \boldsymbol{p}_{b,i} B_i^7\left(\frac{2t-\tau_0-\tau_1}{\Delta\tau_0}\right), \\
\boldsymbol{h}(t) &= \begin{cases} \boldsymbol{h}_a(t), & t \in \left[\tau_0, \frac{\Delta\tau_0}{2}\right) \\ \boldsymbol{h}_b(t), & t \in \left[\frac{\Delta\tau_0}{2}, \tau_1\right], \end{cases} \quad \boldsymbol{h}_a(t) = \sum_{i=0}^{6} \boldsymbol{h}_{a,i} B_i^6\left(\frac{2t-2\tau_0}{\Delta\tau_0}\right), \quad \boldsymbol{h}_b(t) = \sum_{i=0}^{6} \boldsymbol{h}_{b,i} B_i^6\left(\frac{2t-\tau_0-\tau_1}{\Delta\tau_0}\right), \\
\mathcal{A}(t) &= \begin{cases} \mathcal{A}_a(t), & t \in \left[\tau_0, \frac{\Delta\tau_0}{2}\right) \\ \mathcal{A}_b(t), & t \in \left[\frac{\Delta\tau_0}{2}, \tau_1\right], \end{cases} \quad \mathcal{A}_a(t) = \sum_{i=0}^{3} \mathcal{A}_{a,i} B_i^3\left(\frac{2t-2\tau_0}{\Delta\tau_0}\right), \quad \mathcal{A}_b(t) = \sum_{i=0}^{3} \mathcal{A}_{b,i} B_i^3\left(\frac{2t-\tau_0-\tau_1}{\Delta\tau_0}\right),
\end{aligned} \tag{11}$$

where in addition we require that the preimage $\mathcal{A}$ is C^2 continuous at $t = \frac{\tau_0+\tau_1}{2}$. This super-smoothness of order 2 at the joint parameter (instead of G^1 continuity) conceals the effect of the artificial splitting inside the interval and significantly reduces the number of degrees of freedom. Namely, the preimage Bézier coefficients are connected as

$$\mathcal{A}_{a,3} = \mathcal{A}_{b,0} = \frac{1}{4}\left(\mathcal{A}_{a,1} + 2\mathcal{D} + \mathcal{A}_{b,2}\right), \quad \mathcal{A}_{a,2} = \frac{1}{2}\left(\mathcal{A}_{a,1} + \mathcal{D}\right), \quad \mathcal{A}_{b,1} = \frac{1}{2}\left(\mathcal{A}_{b,2} + \mathcal{D}\right) \tag{12}$$

for some $\mathcal{D} \in \mathbb{A}$, see Fig. 1 ($\mathcal{D}$, $\mathcal{A}_{a,2}$, $\mathcal{A}_{a,3} = \mathcal{A}_{b,0}$, $\mathcal{A}_{a,2}$, and $\mathcal{A}_{b,1}$ are denoted with a red circle). Note that imposing super-smoothness of order 3 instead of 2 on the preimage would imply that $\mathcal{A}$ is a polynomial curve, and the interpolation problem would coincide with the one considered in Section 3.2. Note further that the C^2 continuous preimage $\mathcal{A}$ implies that the MPH biarc curve $\boldsymbol{p}$ is C^3 continuous at a joint point provided that $\boldsymbol{p}_{a,7} = \boldsymbol{p}_{b,0}$.

The interpolation conditions (10a) (for $j = 0$) are satisfied iff $\boldsymbol{p}_{a,0} = \boldsymbol{P}_0$, $\boldsymbol{p}_{b,7} = \boldsymbol{P}_1$, and

$$\mathcal{A}_{a,0} = \lambda_0\, \mathcal{U}_0, \quad \mathcal{A}_{a,1} = \mu_0\, \mathcal{U}_0 + \frac{\Delta\tau_0}{6}\lambda_0^3\, \mathcal{V}_0, \quad \mathcal{A}_{b,2} = \mu_1\, \mathcal{U}_1 - \frac{\Delta\tau_0}{6}\lambda_1^3\, \mathcal{V}_1, \quad \mathcal{A}_{b,3} = \lambda_1\, \mathcal{U}_1, \tag{13}$$

(see the blue circle points in Fig. 1) which together with (12) prescribes all the coefficients of $\mathcal{A}$ in dependence of $\mathcal{D} \in \mathbb{A}$ and scalar parameters $\lambda_0, \lambda_1, \mu_0, \mu_1$. It remains to fulfill the condition (10b) (for $j = 0$) and the condition $\boldsymbol{p}_{a,7} = \boldsymbol{p}_{b,0}$. The later is, by applying (5) for $\boldsymbol{p}_a$ and $\boldsymbol{p}_b$ with $i = 6$ and $\Delta\tau = \frac{\Delta\tau_0}{2}$, equal to

$$\boldsymbol{P}_0 + \frac{\Delta\tau_0}{14}\sum_{j=0}^{6} \boldsymbol{h}_{a,j} = \boldsymbol{P}_1 - \frac{\Delta\tau_0}{14}\sum_{j=0}^{6} \boldsymbol{h}_{b,j},$$

which by further applying (4) (for $\boldsymbol{h}_a$ and $\boldsymbol{h}_b$), (12) and (13) reduces to

$$\Delta \boldsymbol{P}_0 = \frac{\Delta\tau_0}{14}\left(\frac{13}{10}\mathcal{D}^{2\star} + \frac{1}{40}\mathcal{D}\star\widetilde{\mathcal{E}} + \frac{1}{720}\widetilde{\boldsymbol{e}}\right), \tag{14}$$

where

$$\begin{aligned}
\widetilde{\mathcal{E}} &= \left(10\lambda_0 + 78\mu_0\right)\mathcal{U}_0 + \left(10\lambda_1 + 78\mu_1\right)\mathcal{U}_1 + 13\Delta\tau_0\lambda_0^3\mathcal{V}_0 - 13\Delta\tau_0\lambda_1^3\mathcal{V}_1,\\
\widetilde{\boldsymbol{e}} &= \kappa_1(\lambda_0,\mu_0)\,\mathcal{U}_0^{2\star} + \kappa_1(\lambda_1,\mu_1)\,\mathcal{U}_1^{2\star} + \kappa_2(\lambda_0,\mu_0)\,\mathcal{U}_0\star\mathcal{V}_0 - \kappa_2(\lambda_1,\mu_1)\,\mathcal{U}_1\star\mathcal{V}_1 - \kappa_3(\lambda_0,\lambda_1,\mu_0)\,\mathcal{U}_0\star\mathcal{V}_1\\
&\quad + \kappa_3(\lambda_1,\lambda_0,\mu_1)\,\mathcal{U}_1\star\mathcal{V}_0 + \kappa_4(\lambda_0,\lambda_1,\mu_0,\mu_1)\,\mathcal{U}_0\star\mathcal{U}_1 + 31\Delta\tau_0^2\lambda_0^6\,\mathcal{V}_0^{2\star} + 31\Delta\tau_0^2\lambda_1^6\,\mathcal{V}_1^{2\star} - 14\Delta\tau_0^2\lambda_0^3\lambda_1^3\,\mathcal{V}_0\star\mathcal{V}_1,
\end{aligned}$$

and

$$\begin{aligned}
&\kappa_1(\lambda,\mu) := 882\lambda\mu + 720\lambda^2 + 1116\mu^2, \quad \kappa_2(\lambda,\mu) := \Delta\tau_0\left(372\lambda^3\mu + 147\lambda^4\right),\\
&\kappa_3(\lambda_0,\lambda_1,\mu) := \Delta\tau_0\left(84\lambda_1^3\mu + 3\lambda_0\lambda_1^3\right), \quad \kappa_4(\lambda_0,\lambda_1,\mu_0,\mu_1) := 18\lambda_1\mu_0 + 18\lambda_0\mu_1 + 504\mu_1\mu_0.
\end{aligned}$$

By denoting

$$\mathcal{E} = \tfrac{1}{104}\widetilde{\mathcal{E}}, \quad \boldsymbol{e} = \mathcal{E}^{2\star} - \tfrac{1}{936}\widetilde{\boldsymbol{e}} + \tfrac{140}{13\Delta\tau_0}\Delta\boldsymbol{P}_0, \tag{15}$$

Eq. (14) equals $(\mathcal{D} + \mathcal{E})^{2\star} = \boldsymbol{e}$ and has, by Lemma 1, solutions (of four types)

$$\mathcal{D} = \sqrt[\star]{\boldsymbol{e}}\,\mathcal{W}(\ell,\phi) - \mathcal{E}, \quad \ell = 1,2,3,4, \tag{16}$$

depending on an additional free parameter $\phi \in \mathbb{R}$. This provides a closed-form solution for constructing the biarc MPH G^2 interpolant of degree 7 expressed in terms of five free parameters λ_0, λ_1, μ_0, μ_1 and ϕ.

It remains to fulfill the Minkowski length constraint $\mathrm{length}_{\mathrm{M}}(\boldsymbol{p};[\tau_0,\tau_1]) = \Delta L_0$ for some chosen ΔL_0. Since we have assumed that $N(\mathcal{U}_j) > 0$ and we want to construct regular MPH biarc, the length constraint gives one nonlinear scalar equation

$$\Delta L_0 = \frac{\Delta\tau_0}{14}\sum_{j=0}^{6}\left(\sigma_{a,j} + \sigma_{b,j}\right), \tag{17}$$

where $\sigma_{a,j}$ and $\sigma_{b,j}$ are the Bernstein coefficients of $N(\mathcal{A}_a)$ and $N(\mathcal{A}_b)$ (parameterized on $[\tau_0, \tau_0 + \Delta\tau_0]$ and $[\tau_0 + \Delta\tau_0, \tau_1]$ respectively). The following lemma provides a significantly simpler form of Eq. (17), which shows that the length constraint is independent of the parameter ϕ.

Lemma 3. *The length interpolation equation (17) reduces to*

$$\|\boldsymbol{e}\|_{\mathrm{M}}^2 = g^2, \tag{18}$$

where

$$\begin{aligned}
g &:= N(\mathcal{E}) - \tfrac{1}{936}\widetilde{g} + \tfrac{140}{13\Delta\tau_0}\Delta L_0, \qquad (19)\\
\widetilde{g} &:= \kappa_1(\lambda_0,\mu_0)\,N(\mathcal{U}_0) + \kappa_1(\lambda_1,\mu_1)\,N(\mathcal{U}_1) + \kappa_2(\lambda_0,\mu_0)\,N(\mathcal{U}_0,\mathcal{V}_0) - \kappa_2(\lambda_1,\mu_1)\,N(\mathcal{U}_1,\mathcal{V}_1)\\
&\quad - \kappa_3(\lambda_0,\lambda_1,\mu_0)\,N(\mathcal{U}_0,\mathcal{V}_1) + \kappa_3(\lambda_1,\lambda_0,\mu_1)\,N(\mathcal{U}_1,\mathcal{V}_0) + \kappa_4(\lambda_0,\lambda_1,\mu_0,\mu_1)\,N(\mathcal{U}_0,\mathcal{U}_1)\\
&\quad + 31\Delta\tau_0^2\lambda_0^6\,N(\mathcal{V}_0) + 31\Delta\tau_0^2\lambda_1^6\,N(\mathcal{V}_1) - 14\Delta\tau_0^2\lambda_0^3\lambda_1^3\,N(\mathcal{V}_0,\mathcal{V}_1),
\end{aligned}$$

and $\boldsymbol{e}$, $\mathcal{E}$ are given by (15). Both g and $\boldsymbol{e}$ depend on the given data and on the parameters λ_0, λ_1, μ_0, μ_1, but not on ϕ. Moreover we associate with every solution of (18) the index set $I = \{1,2\}$ or $I = \{3,4\}$ in the following way. If $(\|\boldsymbol{e}\|_{\mathrm{M}} = g) \wedge (\alpha(\boldsymbol{e}) \le 0)$ or $(\|\boldsymbol{e}\|_{\mathrm{M}} = -g) \wedge (\alpha(\boldsymbol{e}) > 0)$ take $I = \{1,2\}$, else take $I = \{3,4\}$. These sets define for every solution of (18) the admissible choice of indices ℓ in (16).

Proof. By some straightforward computations one can see that by applying (6), (12) and (13), Eq. (17) equals

$$\Delta L_0 = \frac{\Delta\tau_0}{14}\left(\frac{13}{10}N(\mathcal{D}) + \frac{1}{40}N(\mathcal{D},\widetilde{\mathcal{E}}) + \frac{1}{720}\widetilde{g}\right),$$

which further simplifies to

$$N(\mathcal{D}) + 2N(\mathcal{D},\mathcal{E}) + \frac{1}{936}\widetilde{g} - \tfrac{140}{13\Delta\tau_0}\Delta L_0 = 0. \tag{20}$$

Using the equality $N(\mathcal{D}+\mathcal{E}) = N(\mathcal{D}) + 2N(\mathcal{D},\mathcal{E}) + N(\mathcal{E})$, Eq. (20) equals $N(\mathcal{D}+\mathcal{E}) - g = 0$. Since $\mathcal{D}+\mathcal{E} = \sqrt[\star]{e}\,\mathcal{W}(\ell,\phi)$ (by (16)) and since

$$N(\sqrt[\star]{e}\,\mathcal{W}(\ell,\phi)) = N(\sqrt[\star]{e})N(\mathcal{W}(\ell,\phi)), \quad N(\mathcal{W}(\ell,\phi)) = \begin{cases} 1, & \ell = 1,2 \\ -1, & \ell = 3,4, \end{cases}$$

Eq. (20) further reduces to two nonlinear equations

$$N(\sqrt[\star]{e}) - g = 0 \quad \text{for} \quad \ell = 1,2, \quad \text{and} \quad N(\sqrt[\star]{e}) + g = 0 \quad \text{for} \quad \ell = 3,4. \tag{21}$$

By Remark 1 we know that $N(\sqrt[\star]{e}) = \pm \|e\|_M$ depending on the sign of $\alpha(e)$. Thus, any solution of (18) provides the solution of one of the equations in (21), and it is straightforward to check the remaining part of the lemma. □

Since the length constraint gives only one scalar equation with four free parameters/unknowns λ_0, λ_1, μ_0, μ_1, we need to fix three of them in advance and then compute the remaining one as the solution of (18).

3.3.1. Choice of free parameters

We propose to choose

$$\lambda_1 = \xi\lambda_0, \quad \mu_0 = \lambda_0, \quad \mu_1 = \xi\lambda_0 \tag{22}$$

for some $\xi > 0$. The arguments for such a suggestion are the following. It is straightforward to see from (13) that ξ^2 prescribes the ratio between Minkowski norms of boundary tangent vectors provided that $\left\|\mathcal{U}_0^{2\star}\right\|_{\mathrm{M}} = \left\|\mathcal{U}_1^{2\star}\right\|_{\mathrm{M}}$. Usually $\xi = 1$ turns out to be a good choice, but other choices can also be considered, according with the data. From Remark 3 we see that choosing $\lambda_{j,1} = \frac{3(\mu_j-\lambda_j)}{\Delta\tau_j} = 0$ implies that the spline second order derivative vectors at τ_j have the same direction as the given second order derivative vectors $\boldsymbol{d}_j = 2\mathcal{U}_j \star \mathcal{V}_j$, i.e., $\boldsymbol{s}''(\tau_j) = \lambda_j^4 \boldsymbol{d}_j$. This implies the suggested choice $\mu_j = \lambda_j$.

After fixing ξ, μ_0 and μ_1, any solution λ_0 of Eq. (18) gives a one-parametric family of interpolating biarcs that depend on the parameter $\phi \in \mathbb{R}$ and index $\ell \in I$. Note that we need to select only the interpolants that are regular, else length constraint may not be fulfilled since Eq. (18) is derived based on this assumption.

The idea behind the selection of the parameter $\phi \in \mathbb{R}$ and index $\ell \in I$ is to bring the biarc as close as possible to the single polynomial MPH interpolant. Since by (13) the preimage biarc is already C^2 continuous, imposing in addition the C^3 continuity at the joint point, which is satisfied if $8\mathcal{A}_{a,3} - 12\mathcal{A}_{a,2} + 6\mathcal{A}_{a,1} - \mathcal{A}_{a,0} - \mathcal{A}_{b,3} = 0$, would imply that the preimage is a subdivision of a single cubic preimage curve and the same would hold true for the biarc MPH curve. As the above equation in general cannot be satisfied, we propose to select ϕ and ℓ using the minimization in L^2 norm

$$(\phi_{\mathrm{opt}}, \ell_{\mathrm{opt}}) = \operatorname*{argmin}_{\phi\in\mathbb{R},\ell=I} F(\phi,\ell), \quad F(\phi,\ell) := \|8\mathcal{A}_{a,3} - 12\mathcal{A}_{a,2} + 6\mathcal{A}_{a,1} - \mathcal{A}_{a,0} - \mathcal{A}_{b,3}\|_2 = \left\|\mathcal{K} - 2\sqrt[\star]{e}\,\mathcal{W}(\ell,\phi)\right\|_2,$$
$$\mathcal{K} := \left(2\mu_0 - \lambda_0\right)\mathcal{U}_0 + \left(2\mu_1 - \lambda_1\right)\mathcal{U}_1 + \tfrac{1}{3}\Delta\tau_0\lambda_0^3\mathcal{V}_0 - \tfrac{1}{3}\Delta\tau_0\lambda_1^3\mathcal{V}_1 + 2\mathcal{E}. \tag{23}$$

Lastly, we need to check if the computed MPH interpolant is indeed regular, i.e., if the Clifford norm of its preimage $N(\mathcal{A}(t))$ has a constant sign for $t \in [\tau_0, \tau_1]$.

Analyzing the existence of the solution of Eq. (18) and the regularity of the computed interpolants for general input data is significantly more complex than for spatial PH curves (see [19, Theorem 2]), because in the Minkowski space $\mathbb{R}^{2,1}$ vectors may not be space-like. Moreover, checking if $N(\mathcal{A}(t))$ maintains a constant sign can be easily done numerically after computing the solution λ_0 and determining ϕ_{opt}, ℓ_{opt}, but an analytical examination of this condition does not seem feasible.

Remark 5. It is straightforward to verify that, for the choice (22), the function $\|e\|_{\mathrm{M}}^2 - g^2$ is even in the variable λ_0. Consequently, the solutions of Eq. (18) occur in symmetric $\pm$ pairs. It suffices to consider only the positive solutions, since the negative ones yield the same MPH interpolants, provided that the sign of ϕ_{opt} is reversed and ℓ_{opt} is chosen from the complement of the index set I.

Remark 6. If there are more (positive) solutions λ_0 of Eq. (18), we finally select among regular interpolants the one for which the value of $F(\phi_{\mathrm{opt}}, \ell_{\mathrm{opt}})$ is minimal.

3.3.2. Algorithmic procedure

The following algorithm summarizes the main steps in the construction of the biarc MPH interpolant.

Algorithm 1. Construction of the biarc MPH interpolant

`Input:` points $\boldsymbol{P}_0, \boldsymbol{P}_1 \in \mathbb{R}^{2,1}$, frame and velocity data $\mathcal{U}_0$, $\mathcal{U}_1$, $\mathcal{V}_0$, $\mathcal{V}_1 \in \mathbb{A}$, length L, parameter ξ

---

set $\lambda_1 = \xi\lambda_0$, $\mu_0 = \lambda_0$, $\mu_1 = \xi\lambda_0$;
define $\mathcal{A}_{a,0}, \mathcal{A}_{a,1}, \mathcal{A}_{b,2}, \mathcal{A}_{b,3}$ (as functions of λ_0) by (13)
define $\boldsymbol{e}$ (as a function of λ_0) by (15);
define g (as a function of λ_0) by (19);
compute real solutions λ_0 of the nonlinear equation (18) and collect the positive ones in the set Λ;
`for each` $\lambda_0 \in \Lambda$
  determine the index set I as described in Lemma 3;
  compute $(\phi_{\text{opt}}, \ell_{\text{opt}})$ by (23);
  compute $\mathcal{D}$ by (16), and $\mathcal{A}_{a,2}, \mathcal{A}_{a,3}, \mathcal{A}_{b,0}, \mathcal{A}_{b,1}$ by (12);
  discard λ_0 from the set Λ if $N(\mathcal{A}(t)) = 0$ for some $t \in [\tau_0, \tau_1]$;
`end for`
`if` $\Lambda \neq \emptyset$
  select among the solutions in Λ the one with the minimal value $F(\phi_{\text{opt}}, \ell_{\text{opt}})$;
  compute the MPH biarc $\boldsymbol{p}$ by (11);
`else` $\boldsymbol{p} = \{\}$

`Output:` biarc $\boldsymbol{p}$

4. Computation of frame data

In this section we propose two different ways of computing the input preimage points $\mathcal{U}_j$ and preimage derivatives $\mathcal{V}_j$, $j = 0, 1, \ldots, J$, that are needed for the construction of G^2 continuous MPH interpolants. In the first approach we suggest a simple way to compute these data only from given points and the first and second order derivative vectors. In the second approach we adopt the *double reflection method* [20] for computing the rotation-minimizing adapted frames of curves in euclidean tridimensional space to the Minkowski space.

4.1. Frame data from the first and the second order derivative vectors

Suppose that the first and the second order derivative vectors $\boldsymbol{t}_j \in \mathbb{R}^{2,1}$ and $\boldsymbol{d}_j \in \mathbb{R}^{2,1}$, $j = 0, 1, \ldots, J$, are given. By Remark 3 these vectors are related to $\mathcal{U}_j \in \mathbb{A}$ and $\mathcal{V}_j \in \mathbb{A}$ through equalities $\mathcal{U}_j^{2\star} = \boldsymbol{t}_j$ and $2\,\mathcal{U}_j \star \mathcal{V}_j = \boldsymbol{d}_j$. Using Lemma 1 we get that $\mathcal{U}_j = \sqrt[\star]{\boldsymbol{t}_j}\,\mathcal{W}(\ell, \psi)$ for some $\ell = 1, 2, 3, 4$ and some $\psi \in \mathbb{R}$. Since we want $N(\mathcal{U}_j) > 0$ for every $j = 0, 1, \ldots, J$, and since $N(\mathcal{W}(1, \cdot)) = N(\mathcal{W}(2, \cdot)) = -N(\mathcal{W}(3, \cdot)) = -N(\mathcal{W}(4, \cdot)) = 1$ we always have only two choices for the index ℓ. We start by prescribing $\mathcal{U}_0 = \sqrt[\star]{\boldsymbol{t}_0}\,\mathcal{W}(1, 0)$ if $N(\sqrt[\star]{\boldsymbol{t}_0}) > 0$, else $\mathcal{U}_0 = \sqrt[\star]{\boldsymbol{t}_0}\,\mathcal{W}(3, 0)$. From $\mathcal{U}_{j-1}$ the next element $\mathcal{U}_j$ is selected (in a least-square sense) so that the L^2 norm between $\mathcal{U}_{j-1}$ and $\mathcal{U}_j$ is minimized:

$$\min_{\psi \in \mathbb{R},\, \ell \in \text{ind}_j} \left\| \sqrt[\star]{\boldsymbol{t}_j}\,\mathcal{W}(\ell, \psi) - \mathcal{U}_{j-1} \right\|_2, \quad \text{where} \quad \text{ind}_j = \begin{cases} \{1, 2\}, & N(\sqrt[\star]{\boldsymbol{t}_j}) > 0, \\ \{3, 4\}, & \text{elsewise.} \end{cases} \tag{24}$$

To determine $\mathcal{V}_j$ from the second order derivative vector $\boldsymbol{d}_j$ we compute, using Lemma 2,

$$\mathcal{V}_j = \frac{1}{2N(\mathcal{U}_j)} \left(\boldsymbol{d}_j + \zeta_j \boldsymbol{e}_{123}\right) \mathcal{U}_j \boldsymbol{e}_1, \tag{25}$$

where we suggest to choose $\zeta_j = 0$. In Section 5 it is numerically shown that this choice gives very good asymptotic results as well as it provides the planarity of data to be preserved.

Remark 7. The derivative vectors $\boldsymbol{t}_j$ are assumed to be space-like. If some $\boldsymbol{t}_j$ would be light-like, i.e., $\left\|\boldsymbol{t}_j\right\|_{\text{M}} = 0$, then it would follow that $N(\sqrt[\star]{\boldsymbol{t}_j}) = N(\mathcal{U}_j) = 0$, and consequently the solution $\mathcal{V}_j$ of the equation $2\,\mathcal{U}_j \star \mathcal{V}_j = \boldsymbol{d}_j$ would not exist. We also note that space-like tangent vectors that are close to being light-like may lead to numerical instability. In particular, according to (25), the components of $\mathcal{V}_j$ can become very large, whereas the components of $\mathcal{U}_j$ remain of moderate size. Large discrepancy in magnitudes may result in loss of numerical precision in subsequent computations. A more detailed stability analysis is beyond the scope of this paper. Nevertheless, the reader should be aware of potential numerical difficulties when working with tangent vectors that are close to light-like.

4.2. Adapted frames for curves in $\mathbb{R}^{2,1}$

Let $\boldsymbol{f} : [i_s, i_e] \to \mathbb{R}^{2,1}$ be a given smooth curve, such that $\|\boldsymbol{f}'(u)\|_{\mathrm{M}} \neq 0$ for any $u \in [i_s, i_e]$, and let $\boldsymbol{t} = \frac{\boldsymbol{f}'}{\|\boldsymbol{f}'\|_{\mathrm{M}}}$ denotes the field of unit tangents of $\boldsymbol{f}$ in the Minkowski space. Moreover, let $\mathcal{Q}(u) = \sqrt[\star]{\boldsymbol{t}(u)} \in \mathbb{A}$, $u \in [i_s, i_e]$, and let

$$\boldsymbol{q}_i(u) = \frac{\mathcal{Q}(u)\boldsymbol{e}_i\overline{\mathcal{Q}}(u)}{N(\mathcal{Q}(u))} = \varrho(u)\mathcal{Q}(u)\boldsymbol{e}_i\overline{\mathcal{Q}}(u), \quad i = 1,2,3, \quad \varrho(u) := N(\mathcal{Q}(u)) = \pm 1,$$

be the orthonormal vectors in $\mathbb{R}^{2,1}$, i.e., $\mathcal{L}(\mathcal{Q}(u)) = (\boldsymbol{q}_1(u), \boldsymbol{q}_2(u), \boldsymbol{q}_3(u)) \in \mathrm{SO}(2,1)$ with the determinant equal to one, where $\mathcal{L}$ is defined in Definition 3. Note that $\boldsymbol{q}_1(u) = \varrho(u)\boldsymbol{t}(u)$, and $\boldsymbol{q}_2(u)$, $\boldsymbol{q}_3(u)$ span the *normal plane* at the point $\boldsymbol{f}(u)$. We say that $\mathcal{L}(\mathcal{Q})$ is the *adapted* Lorentz frame if $\boldsymbol{q}_1 = \boldsymbol{t}$ or equivalently if $\varrho \equiv 1$.

From a chosen scalar function $\psi : [i_s, i_e] \to \mathbb{R}$ and appropriately selected $\ell \in \{1,2,3,4\}$, the frame computed as $\mathcal{F} = \mathcal{L}(\mathcal{Q}\,\mathcal{W}(\ell,\psi))$ is also the adapted Lorentz frame. In more detail,

$$\mathcal{L}(\mathcal{W}(1,\psi)) = \begin{pmatrix} 1 & 0 & 0 \\ 0 & \cosh(2\psi) & \sinh(2\psi) \\ 0 & \sinh(2\psi) & \cosh(2\psi) \end{pmatrix}, \quad \mathcal{L}(\mathcal{W}(2,\psi)) = \mathcal{L}(\mathcal{W}(1,-\psi)),$$

$$\mathcal{L}(\mathcal{W}(3,\psi)) = \begin{pmatrix} -1 & 0 & 0 \\ 0 & \cosh(2\psi) & \sinh(2\psi) \\ 0 & -\sinh(2\psi) & -\cosh(2\psi) \end{pmatrix}, \quad \mathcal{L}(\mathcal{W}(4,\psi)) = \mathcal{L}(\mathcal{W}(3,-\psi)),$$

and the columns of $\mathcal{L}(\mathcal{Q}\,\mathcal{W}(\ell,\psi))$ are equal to

$$\begin{aligned} \boldsymbol{x}_1 &= \varrho_\ell\, \boldsymbol{q}_1 = \varrho_\ell\, \varrho(u)\, \boldsymbol{t}, \\ \boldsymbol{x}_2 &= \boldsymbol{q}_2 \cosh((-1)^{\ell+1}2\psi) + \varrho_\ell\, \boldsymbol{q}_3 \sinh((-1)^{\ell+1}2\psi), \\ \boldsymbol{x}_3 &= \boldsymbol{q}_2 \sinh((-1)^{\ell+1}2\psi) + \varrho_\ell\, \boldsymbol{q}_3 \cosh((-1)^{\ell+1}2\psi), \end{aligned} \tag{26}$$

where $\varrho_\ell = 1$ for $\ell = 1,2$, and $\varrho_\ell = -1$ for $\ell = 3,4$. Thus, it is enough to consider only $\ell = 1$ or $\ell = 3$. If $\varrho(u) = 1$, we need to choose $\ell = 1$, otherwise $\ell = 3$. The following lemma is needed further.

Theorem 2. *Let $\boldsymbol{M} = (\boldsymbol{m}_1, \boldsymbol{m}_2, \boldsymbol{m}_3) \in \mathrm{SO}(2,1)$ be the given matrix with $\det \boldsymbol{M} = 1$. There exists a unique (up to a sign) normalized element $\mathcal{Q} \in \mathbb{A}$, such that $\mathcal{L}(\pm\mathcal{Q}) = \boldsymbol{M}$. It is computed as*

$$\mathcal{Q} = \begin{cases} \mathcal{Q}_0 \mathcal{W}(1,\psi_0), & \langle \boldsymbol{m}_2 + \boldsymbol{m}_3, \boldsymbol{q}_2 \rangle_{\mathrm{M}} > 0 \\ \mathcal{Q}_0 \mathcal{W}(1,\psi_0)\, \boldsymbol{e}_{23}, & \text{elsewise}, \end{cases} \tag{27}$$

where

$$\mathcal{Q}_0 = \begin{cases} \sqrt[\star]{\boldsymbol{m}_1}, & N(\sqrt[\star]{\boldsymbol{m}_1}) > 0 \\ \sqrt[\star]{\boldsymbol{m}_1}\, \mathcal{W}(3,0), & \text{elsewise}, \end{cases} \qquad \boldsymbol{q}_i = \mathcal{Q}_0 \boldsymbol{e}_i \overline{\mathcal{Q}_0},\ i = 1,2,3, \quad \psi_0 = \frac{1}{2} \ln |\langle \boldsymbol{m}_2 + \boldsymbol{m}_3, \boldsymbol{q}_2 \rangle_{\mathrm{M}}|.$$

Proof. Since $N(\mathcal{Q}_0) > 0$ it holds that $\mathcal{L}(\mathcal{Q}_0) = (\boldsymbol{q}_1, \boldsymbol{q}_2, \boldsymbol{q}_3)$, $\boldsymbol{q}_1 = \boldsymbol{m}_1$, and $\mathcal{L}(\mathcal{Q}_0 W(\ell,\psi)) = (\boldsymbol{x}_1, \boldsymbol{x}_2, \boldsymbol{x}_3)$ where $\boldsymbol{x}_i$ are given by (26). Thus we must choose $\ell = 1$ and ψ so that

$$\boldsymbol{m}_2 = \boldsymbol{q}_2 \cosh(2\psi) + \boldsymbol{q}_3 \sinh(2\psi), \quad \boldsymbol{m}_3 = \boldsymbol{q}_2 \sinh(2\psi) + \boldsymbol{q}_3 \cosh(2\psi).$$

Applying the Minkowski scalar product $\langle \cdot, \boldsymbol{q}_2 \rangle_{\mathrm{M}}$ and the summation on these two equations we obtain

$$\langle \boldsymbol{m}_2 + \boldsymbol{m}_3, \boldsymbol{q}_2 \rangle_{\mathrm{M}} = e^{2\psi},$$

which implies $\psi = \psi_0$ provided that $\langle \boldsymbol{m}_2 + \boldsymbol{m}_3, \boldsymbol{q}_2 \rangle_{\mathrm{M}} > 0$. If $\langle \boldsymbol{m}_2 + \boldsymbol{m}_3, \boldsymbol{q}_2 \rangle_{\mathrm{M}} < 0$, then $\mathcal{L}(\mathcal{Q}_0 \mathcal{W}(1,\psi_0)) = (\boldsymbol{m}_1, -\boldsymbol{m}_2, -\boldsymbol{m}_3)$, but $\mathcal{L}(\mathcal{Q}_0 \mathcal{W}(1,\psi_0)\, \boldsymbol{e}_{23}) = (\boldsymbol{m}_1, \boldsymbol{m}_2, \boldsymbol{m}_2)$. It remains to prove that $\langle \boldsymbol{m}_2 + \boldsymbol{m}_3, \boldsymbol{q}_2 \rangle_{\mathrm{M}}$ cannot be zero. Suppose that $\langle \boldsymbol{m}_2 + \boldsymbol{m}_3, \boldsymbol{q}_2 \rangle_{\mathrm{M}} = 0$. Since $\langle \boldsymbol{q}_1, \boldsymbol{q}_2 \rangle_{\mathrm{M}} = 0$, we can write $\boldsymbol{q}_2 = \eta_2 \boldsymbol{m}_2 + \eta_3 \boldsymbol{m}_3$ for some $\eta_2, \eta_3 \in \mathbb{R}$. Then $0 = \langle \boldsymbol{m}_2 + \boldsymbol{m}_3, \boldsymbol{q}_2 \rangle_{\mathrm{M}} = \eta_2 - \eta_3$ implies $\eta_2 = \eta_3$, but on the other hand $\pm 1 = \langle \boldsymbol{q}_2, \boldsymbol{q}_2 \rangle_{\mathrm{M}} = \eta_2^2 - \eta_3^2$, which is a contradiction. This completes the proof. □

For curves in the euclidean tridimensional space an ideal adapted frame is the rotation minimizing frame (RMF), characterized by the property that the normal frame vectors have no instantaneous rotation about the tangent vector. However, in general the RMF cannot be computed exactly and therefore one often needs to approximate the exact RMF by a sequence of orthonormal frames at sampled points on the given curve. A simple and efficient method, called the *double reflection method* is presented in [20]. Here we adapt it to curves in Minkowski space by replacing the euclidean scalar and vector products with the Minkowski ones (see Algorithm 2). As it is illustrated in Section 5 (Numerical examples), the method works very well. However, more precise definition and the theoretical analysis is beyond the scope of this paper and is left to a future research.

Algorithm 2. Computation of rotation minimizing Lorentz frame vectors

Input: sequence of data points $\boldsymbol{P}_j$ and unit tangent vectors $\boldsymbol{t}_j$ $j = 0, 1, \dots, N$.

```
Q_0 = ⋆√t_0
if N(Q_0) < 0 then Q_0 = Q_0 W(3,0)
F_0 = (t_0, r_0, s_0) = L(Q_0)
for j = 0, 1, ..., N − 1
    v_1 = P_{j+1} − P_j
    c_1 = ⟨v_1, v_1⟩_M
    r_j^L = r_j − (2/c_1) ⟨v_1, r_j⟩_M v_1
    t_j^L = t_j − (2/c_1) ⟨v_1, t_j⟩_M v_1
    v_2 = t_{j+1} − t_j^L
    c_2 = ⟨v_2, v_2⟩_M
    r_{j+1} = r_j^L − (2/c_2) ⟨v_2, r_j^L⟩_M v_2
    s_{j+1} = t_{j+1} ×_M r_{j+1},
    F_{j+1} = (t_{j+1}, r_{j+1}, s_{j+1})
end for
```

Output: $\mathcal{F}_j$, $j = 0, 1, \dots, N$

Algorithm 2 returns the sequence of frames provided that the values c_1 and c_2 are nonzero at each loop-step of the algorithm. Thus, to equip the given curve $\boldsymbol{f}$ with the approximate (discrete) RMF Lorentz frame, we choose the set of equidistant parameters $u_k = i_s + kh$, $h = \frac{i_e - i_s}{N}$, $k = 0, 1, \dots, N$, for some chosen $N \in \mathbb{N}$, compute points $\boldsymbol{f}(u_k)$ and unit tangent vectors $\boldsymbol{t}_k = \boldsymbol{t}(u_k)$, $k = 0, 1, \dots, N$, and apply Algorithm 2 to get the sequence of frames $\mathcal{F}_k \in \mathrm{SO}(2,1)$, $k = 0, 1, \dots, N$. Furthermore, using Theorem 2 we compute for each $\mathcal{F}_k$ the $\mathcal{Q}_k \in \mathbb{A}$, such that $\mathcal{L}(\pm\mathcal{Q}_k) = \mathcal{F}_k$, and determine the preimage point $\mathcal{U}_k = \pm\sqrt{\|\boldsymbol{f}'(u_k)\|_{\mathrm{M}}}\mathcal{Q}_k$, where the sign is chosen based on the smaller L^2 distance of $\pm\mathcal{U}_k$ from $\mathcal{U}_{k-1}$. Lastly, for the frame velocity data $\mathcal{V}_k$ we suggest to use (25) with $\zeta_k = 0$.

For the input interpolation data we now choose $N = JK$ for some $K \in \mathbb{N}$ and set $\boldsymbol{P}_j = \boldsymbol{f}(u_{jK})$, $\mathcal{U}_j = \mathcal{U}_{jK}$ and $\mathcal{V}_j = \mathcal{V}_{jK}$, $j = 0, 1, \dots, J$.

5. Numerical examples

In this section we apply our method to several examples to illustrate its effectiveness for different data configurations. Note that the length of the spline interpolant equals $L = \sum_{j=0}^{J-1} \Delta L_j$, so in the case of only one biarc segment we use the notation $L = \Delta L_0$. In all the examples, the solution is obtained within a few milliseconds using a standard laptop.

Example 5.1. We consider the data points and tangents from Example 4.1 of [15], where we add second order derivatives

$$\boldsymbol{P}_0 = \left(\tfrac{1}{2}, \tfrac{4}{5}, \tfrac{1}{10}\right), \ \boldsymbol{P}_1 = \left(-\tfrac{2}{5}, \tfrac{1}{10}, \tfrac{1}{4}\right), \ \boldsymbol{t}_0 = \left(-\tfrac{4}{5}, \tfrac{11}{10}, \tfrac{1}{2}\right), \ \boldsymbol{t}_1 = \left(-\tfrac{9}{10}, -2, \tfrac{1}{2}\right), \ \boldsymbol{d}_0 = (1, 2, 0), \ \boldsymbol{d}_1 = (0, 2, 1).$$

Applying (24) and (25) (with $\zeta_0 = \zeta_1 = 0$) we compute

$$\begin{aligned}
\mathcal{U}_0 &= (-0.4821364247, 0, 0, 0, 1.140755960, 0, -0.5185254363, 0),\\
\mathcal{U}_1 &= (0.8256683763, 0, 0, 0, 1.234261073, 0.2530226125, -0.07544913066, 0),\\
\mathcal{V}_0 &= (-1.092427928, 0, 0, 0, -0.06976107473, -0.4099303509, 0.2049651754, 0),\\
\mathcal{V}_1 &= (-0.5603295581, 0, 0, 0, -0.4458989904, 0.2536655596, 0.3118160160, 0).
\end{aligned}$$

Choosing $\tau_0 = 0$, $\tau_1 = 1$, $\xi = 1$ and the length $L = 1.2\,\|\Delta\boldsymbol{P}_0\|_{\mathrm{M}} = 1.356318547$, the length interpolation equation (18) has two solutions $\lambda_0 = 1.577816217$ (solution of $\|e\|_{\mathrm{M}} + g = 0$) and $\lambda_0 = 0.7409296661$ (solution of $\|e\|_{\mathrm{M}} - g = 0$) For the first solution we have that $\alpha(e) = -0.3812415408$ and for the second solution $\alpha(e) = 2.192849963$. This means that $I = \{3, 4\}$ for both solutions. To determine the optimal parameter ϕ_{opt} by (23) we compute the following results

λ_0	ℓ	ϕ_{opt}	$F(\phi_{\mathrm{opt}}, \ell)$
1.577816217	3	−0.6972822202	190.3181231
1.577816217	4	1.120708593	117.5782321
0.7409296661	3	0.01469756578	130.1832100
0.7409296661	4	0.2008998455	4.730642367

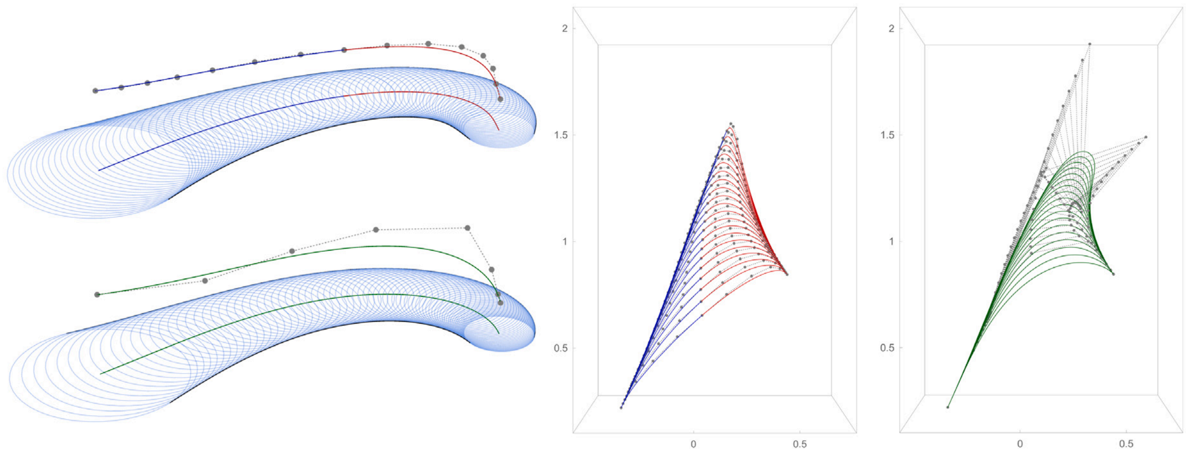

Fig. 2. Left: The biarc (top) and the single polynomial (bottom) G^2 interpolant from Example 5.1 for $L = 1.2\ \|\Delta\boldsymbol{P}_0\|_{\mathrm{M}}$. Middle: Biarc G^2 interpolants of different Minkowski lengths $L = \mathrm{fac}\,\|\Delta\boldsymbol{P}_0\|_{\mathrm{M}}$, $\mathrm{fac} = 1.05, 1.10, 1.15, \ldots, 1.95$. Right: Single polynomial G^2 interpolants of different Minkowski lengths $L = \mathrm{fac}\,\|\Delta\boldsymbol{P}_0\|_{\mathrm{M}}$, $\mathrm{fac} = 1.15, 1.20, 1.25, \ldots, 1.95$.

from which we select $\lambda_0 = 0.7409296661$, $\ell_{\mathrm{opt}} = 4$ and $\phi_{\mathrm{opt}} = 0.2008998455$. The resulting G^2 biarc interpolant together with the control polygon and with the planar domain determined by the medial axis transform is shown in Fig. 2 (top left). The middle plot shows the interpolants for different values of L.

In addition, in order to compare the biarc approach with the single polynomial interpolant (Section 3.2), we compute by using the Newton–Raphson method with starting values $\lambda_0 = \lambda_1 = \mu_0 = \mu_1 = 0.75$, the solution

$$\lambda_0 = 0.3959384542, \quad \lambda_1 = 1.084677582, \quad \mu_0 = 1.139740076, \quad \mu_1 = 0.8206039870$$

to the problem introduced in Section 3.2 for $L = \mathrm{fac}\,\|\Delta\boldsymbol{P}_0\|_{\mathrm{M}}$, $\mathrm{fac} = 1.2$. The curve is shown in Fig. 2 (bottom left) together with the control polygon and with the planar domain determined by the medial axis transform. Following this solution by a homotopy approach as the factor fac is decreasing from 1.2 by a stepsize 0.001, the numerical computations show that the solution vanishes for $\mathrm{fac} = 1.104$. To further check the existence of the solution for a fixed L we generated 1000 randomly chosen starting values in $[-3, 3]^4$ and check if the Newton–Raphson method converges. For $\mathrm{fac} \in \{1.104, 1.10, 1.09, \ldots, 1.05\}$ no solutions have been found. Fig. 2 (right) shows single polynomial G^2 interpolants as the Minkowski length L is changing ($L = \mathrm{fac}\,\|\Delta\boldsymbol{P}_0\|_{\mathrm{M}}$, $\mathrm{fac} = 1.15, 1.20, 1.25, \ldots, 1.95$). One can note that the control polygons are much more distant from the curve as in the case of biarc interpolants.

Example 5.2. This example illustrates the preservation of planarity for appropriately computed input preimage data. The data are taken from Example 1 of [14], where a C^2 construction is considered:

$$\boldsymbol{P}_0 = (0,0,0),\ \boldsymbol{P}_1 = (1,0,0),\ \boldsymbol{t}_0 = (1,1,0),\ \boldsymbol{t}_1 = (2,1,0),\ \boldsymbol{d}_0 = (1,2,0),\ \boldsymbol{d}_1 = (1,2,0).$$

Applying (24) and (25) (with $\zeta_0 = \zeta_1 = 0$) we compute

$$\begin{aligned}
\mathcal{U}_0 &= (-1.098684113, 0, 0, 0, 0.4550898606, 0, 0, 0),\\
\mathcal{U}_1 &= (-1.455346690, 0, 0, 0, 0.3435607497, 0, 0, 0),\\
\mathcal{V}_0 &= (-0.7102406200, 0, 0, 0, 0.6159884238, 0, 0, 0),\\
\mathcal{V}_1 &= (-0.4790704512, 0, 0, 0, 0.5740283070, 0, 0, 0).
\end{aligned}$$

For $\tau_0 = 0$, $\tau_1 = 1$, $\xi = 1$ and the length $L = 1.1$, the optimal solution is obtained for $\lambda_0 = 0.7928050502$, $\ell_{\mathrm{opt}} = 3$ and $\phi_{\mathrm{opt}} = 0$. The G^2 biarc interpolant lies in the plane since the third component of each control point is equal to zero; see Fig. 3 (left). Note that it coincides with the planar G^2 PH interpolant constructed in [18], which interpolates the planar G^2 data, i.e., the data points and unit tangent vectors (with the last component omitted), the curvatures κ_0, κ_1 computed from the input derivative vectors, and the length L, provided that the additional free parameters are chosen appropriately.

The interpolants for different values of L are shown in Fig. 3 (middle). If we choose nonzero values for ζ_0 and ζ_1, e.g., $\zeta_0 = 1$, $\zeta_1 = 10$ we obtain

$$\begin{aligned}
\mathcal{V}_0 &= (-0.7102406200, 0, 0, 0, 0.6159884238, -0.7768869870, -0.3217971265, 0),\\
\mathcal{V}_1 &= (-0.4790704512, 0, 0, 0, 0.5740283070, -6.508508260, -1.536450382, 0),
\end{aligned}$$

and the optimal G^2 interpolant, obtained for $\lambda_0 = 0.8108827137$, $\ell_{\mathrm{opt}} = 3$ and $\phi_{\mathrm{opt}} = 0.2753063093$, is not planar as shown in Fig. 3 (right).

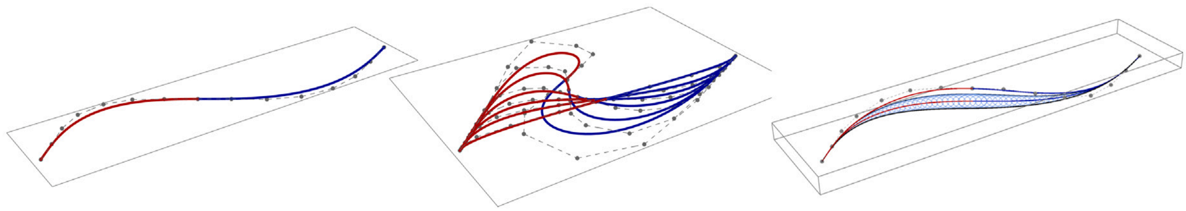

Fig. 3. Left: G^2 interpolant from Example 5.2 for $L = 1.1$ and $\zeta_0 = \zeta_1 = 0$ that preserves the planarity of the input points and derivatives. Middle: Interpolants with different Minkowski lengths $L = 1.01, 1.05, 1.1, 1.2, 1.5, 2$. Right: Nonplanar G^2 interpolant from Example 5.2 for $L = 1.1$ and $\zeta_0 = 1, \zeta_1 = 10$ together with the planar domain determined by the medial axis transform. In all the pictures the two biarc segments are shown in red and blue. (For interpretation of the colors in this figure, the reader is referred to the web version of this article.)

Table 1
Errors of spline interpolants from Example 5.3 for two different choices of input preimage data in dependence of the number of segments J together with decay exponents as J increases.

	CASE 1		CASE 2	
J	error	decay exp.	error	decay exp.
2	$6.7362\cdot 10^{-5}$	/	$4.0630\cdot 10^{-4}$	/
4	$2.2062\cdot 10^{-6}$	4.9323	$4.5800\cdot 10^{-5}$	3.1491
5	$7.7100\cdot 10^{-7}$	4.7115	$2.3428\cdot 10^{-5}$	3.0042
10	$2.2979\cdot 10^{-8}$	5.0684	$2.9519\cdot 10^{-6}$	2.9885
20	$6.6207\cdot 10^{-10}$	5.1172	$3.7091\cdot 10^{-7}$	2.9925
25	$2.1466\cdot 10^{-10}$	5.0476	$1.9006\cdot 10^{-7}$	2.9963

In the remaining examples we sample the data from a chosen curve $\boldsymbol{f} : [i_s, i_e] \to \mathbb{R}^{2,1}$, such that $\|\boldsymbol{f}'(u)\|_{\mathrm{M}} \neq 0$ for any $u \in [i_s, i_e]$, and observe asymptotic properties of the derived G^2 spline interpolants. To measure the error between the curve segment $\{\boldsymbol{f}(u); u \in [u_j, u_{j+1}]\}$, $i_s \le u_j < u_{j+1} \le i_e$, and a spline biarc segment $\{\boldsymbol{s}(t); t \in [\tau_j, \tau_{j+1}]\}$, we reparameterize $\boldsymbol{f}$ by a function $\varphi : [\tau_j, \tau_{j+1}] \to [u_j, u_{j+1}]$, such that

$$\varphi(\tau_j) = u_j, \quad \varphi(\tau_{j+1}) = u_{j+1}, \quad \varphi'(\tau_j) = \lambda_0^2, \quad \varphi'(\tau_{j+1}) = \lambda_1^2, \quad \varphi''(\tau_j) = \varphi''(\tau_{j+1}) = 0, \tag{28}$$

to achieve $\boldsymbol{s}^{(k)}(\tau_j) = \frac{d^k(\boldsymbol{f}\circ\varphi)}{dt^k}(\tau_j)$ and $\boldsymbol{s}^{(k)}(\tau_{j+1}) = \frac{d^k(\boldsymbol{f}\circ\varphi)}{dt^k}(\tau_{j+1})$ for $k = 0, 1, 2$, and compute

$$E_{\mathrm{err}} = \max_{t\in[\tau_j,\tau_{j+1}]} \|\boldsymbol{s}(t) - (\boldsymbol{f}\circ\varphi)(t)\|_2. \tag{29}$$

Note that we use here the euclidean and not the Minkowski norm as we are interested in the difference between curves observed as curves in a 3D space.

Example 5.3. Let $\boldsymbol{f} : [0, 1] \to \mathbb{R}^{2,1}$, $\boldsymbol{f}(u) = \left(\cos(4u) - 1, \sin(4u), \frac{1}{4}\sqrt{1 + 4u^2}\right)$ be a given curve. Using Algorithm 2 with $N = 100$ we compute a sequence of frames $\mathcal{F}_k \in \mathrm{SO}(2,1)$ and the corresponding preimage points $\mathcal{U}_k$, $k = 0, 1, \ldots, N$. The frame velocity data $\mathcal{V}_k$ are computed by (25) with $\zeta_k = 0$ for each k. The curve $\boldsymbol{f}$ together with frame vectors is shown in Fig. 4 (left). For the number of spline segments we choose $J \in \{2, 4, 5, 10, 20, 25\}$, we select $\tau_j = j$, $j = 0, 1, \ldots, J$, and take the data to be interpolated as

$$\boldsymbol{f}(i_s + j(i_e - i_s)/J), \quad \mathcal{U}_{jN/J}, \quad \mathcal{V}_{jN/J}, \quad j = 0, 1, \ldots, J.$$

The lengths on every segment are determined by the Minkowski length of the curve $\boldsymbol{f}$ on $[u_j, u_{j+1}]$. Fig. 4 (right) shows the resulting G^2 spline interpolant for $J = 5$ together with the planar domain determined by the medial axis transform. The errors together with a decay exponent, i.e., numerical estimate of the approximation order, given in Table 1 (first column — CASE 1), indicate that the approximation order is five, which is the optimal order to be expected for G^2 (biarc) spline interpolants. The second column (CASE 2) shows the errors if we compute for each spline interpolant the input preimage data from the first and second order derivatives of $\boldsymbol{f}$ using (24) and (25) (with $\zeta_j = 0$). In this case the approximation order equals three.

Example 5.4. In this example we choose the curve $\boldsymbol{f} : [0, 1] \to \mathbb{R}^{2,1}$, see [13]

$$\boldsymbol{f}(u) = \left(\frac{12}{10}u, \frac{1}{4}u\sin(8u - 1), 1 - \cosh\left(u - \frac{1}{2}\right)/\cosh\left(\frac{1}{2}\right)\right)$$

and compute the input data in the same way as in the previous example for $J \in \{2, 4, 5, 10, 20, 25\}$. The curve $\boldsymbol{f}$, together with the frame vectors, obtained by Algorithm 2, is shown in Fig. 5 (left). Fig. 5 (right) shows the resulting G^2 spline interpolant for $J = 5$ together with the planar domain determined by the medial axis transform. From Table 2, which shows the approximation errors and decay exponents, we see that the asymptotic behavior of the method is the same as in Example 5.3.

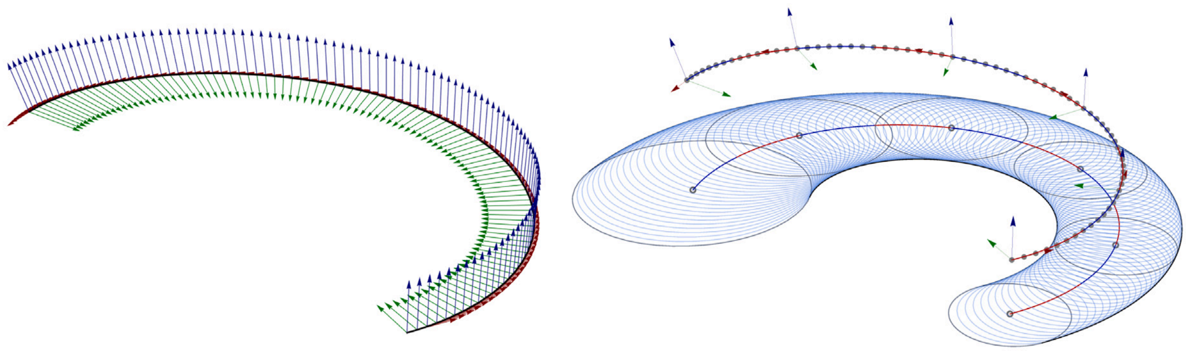

Fig. 4. Left: Curve f from Example 5.3 equipped with Lorentz frame vectors computed by Algorithm 2. Right: G^2 spline interpolant for $J = 5$ together with the planar domain determined by the medial axis transform.

Table 2
Errors of spline interpolants from Example 5.4 for two different choices of input preimage data in dependence of the number of segments J together with decay exponents as J increases.

J	CASE 1		CASE 2	
	error	xdecay exp.	error	decay exp.
2	$7.0790 \cdot 10^{-3}$	/	$5.1521 \cdot 10^{-3}$	/
4	$8.4684 \cdot 10^{-4}$	3.0634	$8.3997 \cdot 10^{-4}$	2.6168
5	$7.5400 \cdot 10^{-4}$	0.52040	$8.1115 \cdot 10^{-4}$	0.15646
10	$1.5464 \cdot 10^{-5}$	5.6076	$1.4043 \cdot 10^{-5}$	5.8520
20	$5.9048 \cdot 10^{-7}$	4.7109	$2.0811 \cdot 10^{-6}$	2.7545
25	$1.8848 \cdot 10^{-7}$	5.1175	$9.7257 \cdot 10^{-7}$	3.4089

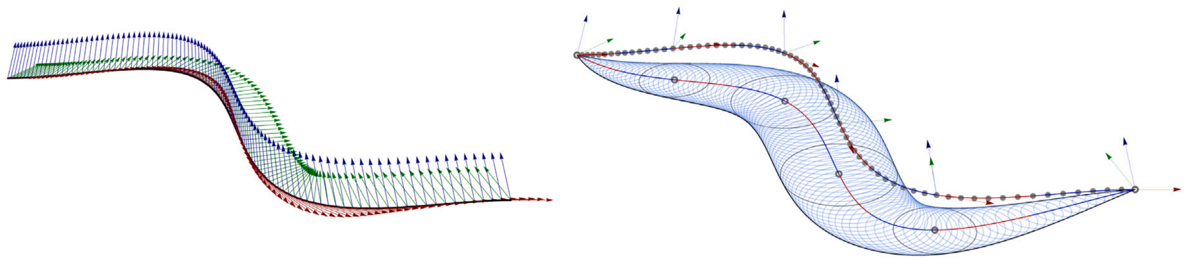

Fig. 5. Left: Curve f from Example 5.4 equipped with Lorentz frame vectors computed by Algorithm 2. Right: G^2 spline interpolant for $J = 5$ together with the planar domain determined by the medial axis transform.

Example 5.5. Suppose now that the points and the derivatives are sampled from the curve

$$f(u) = \left(3\sqrt{u+0.1}\cos(5\pi u), 3\sqrt{u+0.1}\sin(5\pi u), \tfrac{1}{8}\sin(8\pi u) + 0.2\right), \quad u \in [0,1],$$

at equidistant parameters $u_j = j/6$, $j = 0, 1, \ldots, 6$, and that the preimage data are computed using Algorithm 2 with $N = J = 6$. When ΔL_j is taken as the Minkowski length of each curve segment, the approximation error equals $5.2681 \cdot 10^{-3}$. Fig. 6 shows the obtained G^2 spline interpolant (middle), its Lorentz frame (left) and the domain determined by the medial axis transform (right). Further, we choose $\Delta L_j = \mathrm{fac}\left\|f(u_{j+1}) - f(u_j)\right\|_{\mathrm{M}}$ for different factors $\mathrm{fac} \in \{1.1, 1.2, 1.3, 1.4\}$. The domains determined by the medial axis transform of the computed G^2 spline interpolants are shown in Fig. 7.

Example 5.6. As the last example, we choose only the discrete set of data points in the Minkowski space $\mathbb{R}^{2,1}$ and construct the G^2 MPH interpolant. Two sets of data points are considered. The first one is inspired by Example 6.1 of [17]. In order to compute the derivative information that is needed for our method, we compute the well-known cubic C^2 spline interpolant where we fix the boundary first-order derivatives to $(-0.4, 0.04, -0.07)$ and $(-0.06, -0.4, -0.02)$ (sea horse example) $(0.05, 0.2, 0.01)$ and $(0.5, 0.5, -0.3)$ (snake example). The values of the data $\{(x_k, y_k, r_k) : k = 1, \ldots, K\}$ are reported in Fig. 8 together with the resulting domain determined by the medial axis transform of the computed G^2 MPH interpolants for $K = 20$ (left) and $K = 16$ (right).

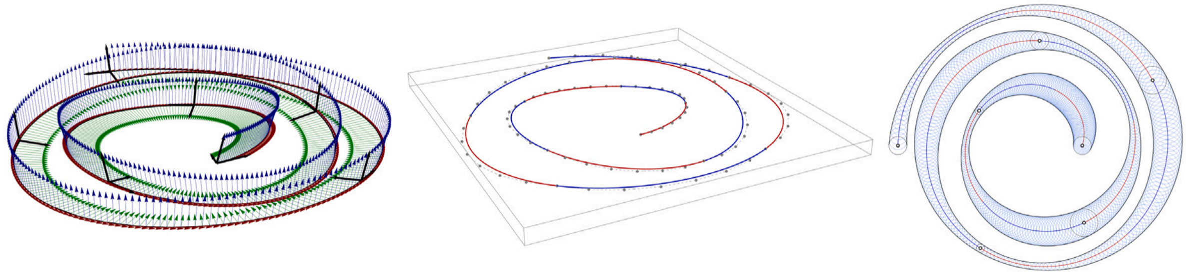

Fig. 6. Left: Curve $\boldsymbol{f}$ from Example 5.5 equipped with Lorentz frame vectors computed by Algorithm 2. Middle: G^2 spline interpolant for $J = 6$, when L_j is taken as the Minkowski length of each curve segment. Right: the planar domain determined by the medial axis transform.

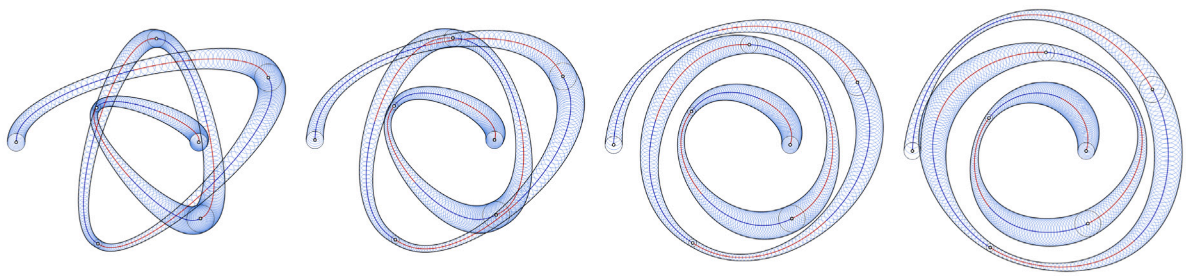

Fig. 7. Several domains determined by the medial axis transform for the MPH spline interpolants based on the data in Example 5.5 with $\Delta L_j = \mathrm{fac}\left\|\boldsymbol{f}(u_{j+1}) - \boldsymbol{f}(u_j)\right\|_{\mathrm{M}}$, where from left to right $\mathrm{fac} \in \{1.1, 1.2, 1.3, 1.4\}$.

6. Asymptotic analysis

As demonstrated by the numerical examples in Section 5, the proposed G^2 interpolation scheme based on Algorithm 2 achieves fifth-order accuracy. In this section, we present the main steps of the proof of this approximation order, which is based on Taylor expansions computed using `Wolfram Mathematica`. Similarly as in [13], we observe the approximation of a curve segment $\boldsymbol{f} : [0, h] \to \mathbb{R}^{2,1}$, such that $\left\|\boldsymbol{f}'(u)\right\|_{\mathrm{M}} \neq 0$ for any $u \in [0, h]$, and analyze the existence and the behavior of solutions for decreasing step-size $h \to 0$. We may assume that the curve is parameterized by its arc length, i.e., $\left\|\boldsymbol{f}'(u)\right\|_{\mathrm{M}} \equiv 1$, and we position the curve so that its Taylor expansion around $u = 0$, which follows using the Frenet formulas (see [13] for the details), equals

$$\begin{aligned}\boldsymbol{f}(u) = \Big(&u - \tfrac{1}{6}\tilde\kappa_0^2 u^3 - \tfrac{1}{8}\tilde\kappa_0\tilde\kappa_1 u^4 + \tfrac{1}{120}\left(\tilde\kappa_0^4 - \tilde\tau_0^2\tilde\kappa_0^2 - 4\tilde\kappa_2\tilde\kappa_0 - 3\tilde\kappa_1^2\right)u^5,\\ &\tfrac{1}{2}\tilde\kappa_0 u^2 + \tfrac{1}{6}\tilde\kappa_1 u^3 + \tfrac{1}{24}\left(-\tilde\kappa_0^3 + \tilde\tau_0^2\tilde\kappa_0 + \tilde\kappa_2\right)u^4 + \tfrac{1}{120}\left(-6\tilde\kappa_1\tilde\kappa_0^2 + 3\tilde\tau_0\tilde\tau_1\tilde\kappa_0 + 3\tilde\kappa_1\tilde\tau_0^2 + \tilde\kappa_3\right)u^5,\\ &\tfrac{1}{6}\tilde\kappa_0\tilde\tau_0 u^3 + \tfrac{1}{24}\left(2\tilde\kappa_1\tilde\tau_0 + \tilde\kappa_0\tilde\tau_1\right)u^4 + \tfrac{1}{120}\left(-\tilde\tau_0\tilde\kappa_0^3 + \tilde\tau_0^3\tilde\kappa_0 + \tilde\tau_2\tilde\kappa_0 + 3\tilde\kappa_2\tilde\tau_0 + 3\tilde\kappa_1\tilde\tau_1\right)u^5\Big)^T + \mathcal{O}\left(u^6\right),\end{aligned}$$

where $\tilde\kappa(u) = \tilde\kappa_0 + \tilde\kappa_1 u + \frac{1}{2!}\tilde\kappa_2 u^2 + + \frac{1}{3!}\tilde\kappa_3 u^3 + \mathcal{O}(u^4)$ and $\tilde\tau(u) = \tilde\tau_0 + \tilde\tau_1 u + \frac{1}{2!}\tilde\tau_2 u^2 + \frac{1}{3!}\tilde\tau_3 u^3 + \mathcal{O}(u^4)$ are the Minkowski curvature and torsion. From data points $\boldsymbol{f}(0)$, $\boldsymbol{f}(h)$ and the corresponding unit tangent vectors we compute by Algorithm 2 the two frames $\mathcal{F}_0$ and $\mathcal{F}_1$, from which we determine $\mathcal{U}_0$, $\mathcal{V}_0$, $\mathcal{U}_1$ and $\mathcal{V}_1$ as described in Section 4.2. Their expansion equals

$$\begin{aligned}\mathcal{U}_0 &= (-1, 0, 0, 0, 0, 0, 0, 0), \quad \mathcal{V}_0 = (0, 0, 0, 0, \tfrac{\tilde\kappa_0}{2}, 0, 0, 0),\\ \mathcal{U}_1 &= (-1 + \tfrac{h^2}{8}\tilde\kappa_0^2 + \tfrac{h^3}{8}\tilde\kappa_0\tilde\kappa_1 + \tfrac{h^4}{384}\left(4\tilde\kappa_0^2\tilde\tau_0^2 - \tilde\kappa_0^4 + 16\tilde\kappa_2\tilde\kappa_0 + 12\tilde\kappa_1^2\right), 0, 0, 0, h\tfrac{\tilde\kappa_0}{2} + \tfrac{h^2}{4}\tilde\kappa_1 +\\ &\quad \tfrac{h^3}{48}\left(4\tilde\kappa_0\tilde\tau_0^2 - \tilde\kappa_0^3 + 4\tilde\kappa_2\right) + \tfrac{h^4}{96}\left(6\tilde\kappa_0\tilde\tau_0\tilde\tau_1 + 6\tilde\kappa_1\tilde\tau_0^2 - 3\tilde\kappa_1\tilde\kappa_0^2 + 2\tilde\kappa_3\right), \tfrac{h^3}{24}\tilde\kappa_0^2\tilde\tau_0 + \tfrac{h^4}{48}\tilde\kappa_0\left(2\tilde\kappa_1\tilde\tau_0 + \tilde\kappa_0\tilde\tau_1\right),\\ &\quad -\tfrac{h^2}{4}\tilde\kappa_0\tilde\tau_0 - \tfrac{h^3}{12}\left(2\tilde\kappa_1\tilde\tau_0 + \tilde\kappa_0\tilde\tau_1\right) + \tfrac{h^4}{96}\left(\tilde\kappa_0^3\tilde\tau_0 - 2\tilde\kappa_0\tilde\tau_0^3 - 2\tilde\kappa_0\tilde\tau_2 - 6\tilde\kappa_2\tilde\tau_0 - 6\tilde\kappa_1\tilde\tau_1\right), 0) + \mathcal{O}(h^5),\\ \mathcal{V}_1 &= (\tfrac{h}{4}\tilde\kappa_0^2 + \tfrac{3h^2}{8}\tilde\kappa_0\tilde\kappa_1 + \tfrac{h^3}{96}\left(4\tilde\kappa_0^2\tilde\tau_0^2 - \tilde\kappa_0^4 + 16\tilde\kappa_2\tilde\kappa_0 + 12\tilde\kappa_1^2\right), 0, 0, 0, \tfrac{\tilde\kappa_0}{2} + \tfrac{h}{2}\tilde\kappa_1 + \tfrac{h^2}{16}\left(4\tilde\kappa_0\tilde\tau_0^2 - \tilde\kappa_0^3 + 4\tilde\kappa_2\right) +\\ &\quad \tfrac{h^3}{24}\left(6\tilde\kappa_0\tilde\tau_0\tilde\tau_1 + 6\tilde\kappa_1\tilde\tau_0^2 - 3\tilde\kappa_1\tilde\kappa_0^2 + 2\tilde\kappa_3\right), \tfrac{h^2}{8}\tilde\kappa_0^2\tilde\tau_0 + \tfrac{h^3}{12}\tilde\kappa_0\left(2\tilde\kappa_1\tilde\tau_0 + \tilde\kappa_0\tilde\tau_1\right), -\tfrac{h}{2}\tilde\kappa_0\tilde\tau_0 - \tfrac{h^2}{4}\left(2\tilde\kappa_1\tilde\tau_0 + \tilde\kappa_0\tilde\tau_1\right)\\ &\quad + \tfrac{h^3}{24}\left(\tilde\kappa_0^3\tilde\tau_0 - 2\tilde\kappa_0\tilde\tau_0^3 - 2\tilde\kappa_0\tilde\tau_2 - 6\tilde\kappa_2\tilde\tau_0 - 6\tilde\kappa_1\tilde\tau_1\right), 0) + \mathcal{O}(h^4).\end{aligned}$$

The Minkowski length of the curve segment equals h due to arc-length parameterization. Choosing $\xi = 1$ and $\mu_0 = \mu_1 = \lambda_0$, we observe that the unknown λ_0 admits an expansion of the form $\lambda_0 = c_1\sqrt{h} + c_2 h + c_3\sqrt{h}h + c_4 h^2 + c_5\sqrt{h}h^2 + \mathcal{O}(h^3)$. The length interpolation equation (18) then expands as

$$\|\boldsymbol{e}\|_{\mathrm{M}}^2 - g^2 = -\frac{35}{6591}\kappa_0^2\left(34c_1^8 - 410c_1^6 + 1803c_1^4 - 3247c_1^2 + 1820\right)h^4 + \mathcal{O}(h^5), \tag{30}$$

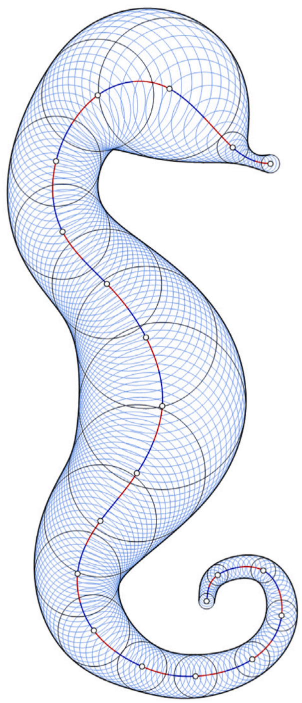

x	y	r
7.91	8.25	0.14
7.33	8.5	0.24
6.36	9.4	1.09
5.26	9.3	0.86
4.62	8.29	0.69
4.72	7.21	0.73
5.4	6.41	0.84
6.	5.59	1.09
6.25	4.54	1.28
5.86	3.51	1.05
5.3	2.78	0.86
4.95	1.97	0.66
5.2	1.1	0.55
5.94	0.55	0.38
6.76	0.4	0.33
7.63	0.66	0.27
8.08	1.33	0.24
7.8	2.02	0.19
7.1	1.95	0.16
6.93	1.55	0.12

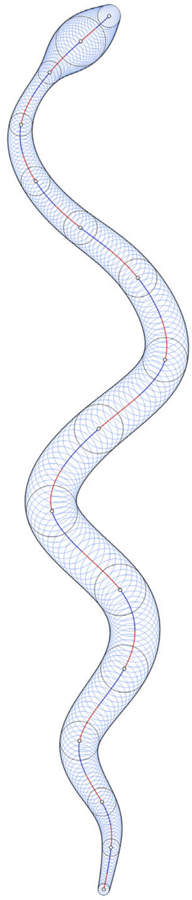

x	y	r
0.03	0.42	0.15
0.22	1.51	0.23
−0.02	2.7	0.37
−0.6	4.29	0.51
0.57	6.17	0.62
0.46	8.22	0.67
−1.32	10.27	0.67
−0.1	12.41	0.64
1.63	14.21	0.58
0.92	16.34	0.5
−0.58	17.65	0.44
−1.75	18.86	0.38
−2.13	20.33	0.3
−1.38	21.69	0.3
−0.57	22.5	0.65
0.17	23.16	0.3

Fig. 8. Two planar domains determined by the medial axis transform of G^2 spline curves, which interpolate, in the MPH sense, the two set of discrete data listed alongside (see Example 5.6 for details).

and has four real solutions $c_1 = \pm 1$ and $c_1 = \pm 2\sqrt{\frac{13}{17}}$, among which, due to Remark 5, it suffices to observe only the positive ones. Since the second solution does not yield optimal asymptotic behavior (the details are omitted here), we restrict our attention to $c_1 = 1$. By observing higher order terms in (30), it follows that $\lambda_0 = \sqrt{h} + \mathcal{O}(h^4)$ with the corresponding index set $\mathcal{I} = \{3, 4\}$. Moreover, from asymptotic expansion of (23) it follows that $\phi_{\text{opt}} = 0$ and $\ell_{\text{opt}} = 3$, which gives

$$\mathcal{D} = \sqrt{h}\,(-1 + \tfrac{h^2}{48}\tilde{\kappa}_0^2, 0, 0, 0, \tfrac{h}{4}\tilde{\kappa}_0 + \tfrac{h^2}{24}\tilde{\kappa}_1, -\tfrac{49h^3}{2496}\tilde{\kappa}_0^2\tilde{\tau}_0, -\tfrac{h^2}{24}\tilde{\kappa}_0\tilde{\tau}_0, 0) + \mathcal{O}(h^{9/2}).$$

The reparameterization function that satisfies (28) equals $\varphi(t) = h\,t + \mathcal{O}(h^6)$ and the error (29) is of the form $E_{\text{err}} = \text{const}(\tilde{\kappa}_0, \tilde{\kappa}_1, \tilde{\kappa}_2, \tilde{\kappa}_3, \tilde{\tau}_0, \tilde{\tau}_1, \tilde{\tau}_2)\,h^5$ proving that the solution $\lambda_0 \simeq \sqrt{h}$ provides the MPH approximant with the approximation order five.

Remark 8. The above analysis of the nonlinear Eq. (30) shows that, in the asymptotic sense, the problem always admits at least one solution. In fact, two solutions exist; however, one of them does not yield satisfactory asymptotic behavior.

7. Conclusions

In this paper we have presented the construction of geometrically continuous MPH spline curves in the Minkowski space $\mathbb{R}^{2,1}$, composed of degree seven polynomial curves, derived from a cubic preimage represented using the Clifford algebra $Cl(2,1)$. These preimage curves are associated with Lorentz orthonormal frames and the connection between geometric continuity of the preimage and that of the resulting curve is revealed. The construction of entirely local interpolating G^2 continuous MPH spline curve accompanied by a G^1 continuous Lorentz frame is examined, under the additional constraint that the Minkowski length of the curve is prescribed. To guarantee the applicability of the proposed scheme to arbitrary interpolation data, each spline segment is constructed as a biarc that connects two polynomial MPH curves and satisfies the prescribed Hermite conditions at the endpoints. Moreover, the preimage of each biarc is C^2 continuous at the junction point of the two consecutive polynomial curves. The proposed approach admits a closed-form solution with additional free parameters, whose selection is guided by various criteria. In addition, two methods for determining the input data in the subspace $\mathbb{A}$ of the Clifford algebra are proposed. The first method requires only discrete information about points and their associated first and second order derivatives. The second introduces a novel approach: it assigns to a given curve in $\mathbb{R}^{2,1}$ a rotation-minimizing Lorentz frame, from which the input data are derived. In particular, the double reflection method — originally developed for curves in Euclidean space — is generalized to the Minkowski setting, and the correspondence between frame vectors and elements of the Clifford algebra subspace $\mathbb{A}$ is established (see Theorem 2). The numerical experiments indicate that the approximation order tends to five when this second method is applied; this approximation order is theoretically confirmed in Section 6.

In addition, the proposed interpolation framework is well suited for CAM applications, in particular for tool-path generation and offset-based machining. The availability of G^2-continuous MPH spline curves with rational offsets allows accurate and stable computation of machining trajectories, while reducing numerical errors in offset evaluation and trimming. The locality of the construction enables efficient modification of individual spline segments, which is advantageous in practical CAM workflows and interactive design environments. Moreover, the prescribed Minkowski length provides additional control on segment spacing, which can be exploited to regulate feed-rate and path parameterization in manufacturing processes.

As a direction for future research, it would be worthwhile to investigate in greater depth the construction, applications, and theoretical properties of rational rotation-minimizing Lorentz frames. While such frames have proven to be highly effective in the context of PH curves in Euclidean space, their potential remains unexplored for MPH curves. We also plan to investigate the L^2 approximation using polynomial MPH curves and MPH B-spline curves (recently introduced in [16]). In this setting, Lorentz frames may offer a promising framework for developing an alternative linearized L^2 approximation method. In addition, extending the ideas and methodologies developed in this paper to the setting of four-dimensional MPH curves in $\mathbb{R}^{3,1}$ presents a challenging direction for further research.

CRediT authorship contribution statement

Marjeta Knez: Writing – review & editing, Writing – original draft, Methodology, Investigation, Formal analysis, Conceptualization. **Francesca Pelosi:** Writing – review & editing, Writing – original draft, Methodology, Investigation, Formal analysis, Conceptualization. **Maria Lucia Sampoli:** Writing – review & editing, Writing – original draft, Methodology, Investigation, Formal analysis, Conceptualization.

Declaration of competing interest

The authors declare that they have no known competing financial interests or personal relationships that could have appeared to influence the work reported in this paper.

Acknowledgments

Research on this paper was supported in part by the research program P1-0288 and grants J1-60011 and N1-0237 from Slovenian Research and Innovation Agency (ARIS), and by INdAM-GNCS, Gruppo Nazionale per il Calcolo Scientifico which F. Pelosi and M.L. Sampoli are members of.

References

[1] R.T. Farouki, T. Sakkalis, Pythagorean hodographs, IBM J. Res. Dev. 34 (5) (1990) 736–752.
[2] R.T. Farouki, Pythagorean-Hodograph Curves: Algebra and Geometry Inseparable, Springer, Berlin, 2008.
[3] R.T. Farouki, C. Giannelli, A. Sestini, New developments in theory, algorithms, and applications for Pythagorean–hodograph curves, in: C. Giannelli, H. Speleers (Eds.), Advanced Methods for Geometric Modeling and Numerical Simulation, in: Springer INdAM Series, 2019, pp. 127–177.
[4] J. Kosinka, M. Lávička, Pythagorean hodograph curves: A survey of recent advances, J. Geom. Graph. 18 (1) (2014) 23–43.
[5] H.P. Moon, Minkowski Pythagorean hodographs, Comput. Aided Geom. Design 16 (1999) 739–753.
[6] H.I. Choi, Ch.Y. Han, H.P. Moon, K.H. Roh, N.S. Wee, Medial axis transform and offset curves by Minkowski Pythagorean hodograph curves, Comput. Aided Des. 31 (1999) 59–72.
[7] H.I. Choi, D.S. Lee, H.P. Moon, Clifford algebra, spin representation and rational parameterization of curves and surfaces, Adv. Comput. Math. 17 (2002) 5–48.
[8] W.L.F. Degen, Exploiting curvatures to compute the medial axis for domains with smooth boundary, Comput. Aided Geom. Design 21 (2004) 641–660.
[9] H. Pottmann, M. Peternell, Applications of Laguerre geometry, Comput. Aided Geom. Design 15 (1997) 165–186.
[10] J. Kosinka, B. Jüttler, C^1 Hermite interpolation by Pythagorean hodograph quintics in Minkowski space, Adv. Comp. Math. 30 (2009) 123–140.
[11] J. Kosinka, M. Lávička, A unified Pythagorean hodograph approach to medial axis transform and offset approximation, J. Comput. Appl. Math. 235 (2011) 3413–3424.
[12] G.I. Kim, M.H. Ahn, C^1 Hermite interpolation using MPH quartic, Comput. Aided Geom. Design 20 (2003) 469–492.
[13] J. Kosinka, B. Jüttler, G^1 Hermite interpolation by Minkowski Pythagorean hodograph cubics, Comput. Aided Geom. Design 23 (2006) 401–418.
[14] J. Kosinka, Z. Šír, C^2 Hermite interpolation by Minkowski Pythagorean hodograph curves and medial axis transform approximation, Comput. Aided Geom. Design 27 (2010) 631–643.
[15] M. Bizzarri, M. Lávička, J. Vršek, Linear computational approach to interpolations with polynomial Minkowski Pythagorean hodograph curves, J. Comput. Appl. Math. 361 (2019) 283–294.
[16] M. Bizzarri, M. Lávička, Construction of Minkowski Pythagorean hodograph B-spline curves, Comput. Aided Geom. Design 80 (2020) 101878.
[17] M. Bizzarri, M. Lávička, Interpolation of Hermite data by clamped Minkowski Pythagorean hodograph B-spline curves, J. Comput. Appl. Math. 392 (2021) 113469.
[18] M. Knez, F. Pelosi, M.L. Sampoli, Construction of G^2 planar Hermite interpolants with prescribed arc lengths, Appl. Math. Comput. 426 (2022) 127092.

[19] M. Knez, F. Pelosi, M.L. Sampoli, Construction of G^2 spatial interpolants with prescribed arc lengths, J. Comput. Appl. Math. 441 (2024) 115684.
[20] W. Wang, B. Jüttler, D. Zheng, Y. Liu, Computation of rotation minimizing frames, Adv. Comp. Math. Trans. Graph. (TOG) 27 (1) (2008) 1–18.
[21] H.I. Choi, S.W. Choi, H.P. Moon, Mathematical theory of medial axis trasform, Pacific J. Math. 181 (1997) 57–88.
[22] G.L. Naber, The Geometry of Minkowski Spacetime, Springer-Verlag, New York, 1992.
[23] M. Knez, M.L. Sampoli, Geometric interpolation of ER frames with G^2 Pythagorean-hodograph curves of degree 7, Comput. Aided Geom. Design 88 (2021) 102001.